AUIQ Technical Engineering Science

Volume 3 | Issue 1 Article 2

2026

Intelligent Coordination Approach for Hybrid Renewable Energy Systems Towards Sustainable Power Supply

Olufisayo Stephen Babalola
Department of Electronic and Electrical Engineering, Faculty of Engineering, Obafemi Awolowo University, Ile-Ife, 220103, babfisayo@gmail.com

Joseph Bukola Samson
Department of Electrical and Electronics Engineering, Faculty of Engineering, Olabisi Onabanjo University, Ago Iwoye, 112104, joseph.samson@oouagoiwoye.edu.ng

Olatunji Waliu Olademeji
Department of Electronic and Electrical Engineering, Faculty of Engineering, Obafemi Awolowo University, Ile-Ife, 220103, waliu2017@gmail.com

Samson Oladayo Ayanlade
Department of Electrical and Electronics Engineering, Faculty of Engineering, Olabisi Onabanjo University, Ago Iwoye, 112104, ayanlade.oladayo@oouagoiwoye.edu.ng

Etinosa Noma-Osaghae
Department of Electrical and Electronics Engineering, Faculty of Engineering, Olabisi Onabanjo University, Ago Iwoye, 112104

Recommended Citation

Babalola, Olufisayo Stephen; Samson, Joseph Bukola; Olademeji, Olatunji Waliu; Ayanlade, Samson Oladayo; Noma-Osaghae, Etinosa; and Ajibola, Opeyemi Ahmed (2026) "Intelligent Coordination Approach for Hybrid Renewable Energy Systems Towards Sustainable Power Supply," *AUIQ Technical Engineering Science*: Vol. 3: Iss. 1, Article 2.
DOI: https://doi.org/10.70645/3078-3437.1053

Intelligent Coordination Approach for Hybrid Renewable Energy Systems Towards Sustainable Power Supply

Authors

Olufisayo Stephen Babalola, Joseph Bukola Samson, Olatunji Waliu Olademeji, Samson Oladayo Ayanlade, Etinosa Noma-Osaghae, and Opeyemi Ahmed Ajibola

AUIQ TECHNICAL ENGINEERING SCIENCE 2026;3:14–45

ORIGINAL STUDY

Intelligent Coordination Approach for Hybrid Renewable Energy Systems Towards Sustainable Power Supply

Olufisayo Stephen Babalola [a], Joseph Bukola Samson [b,*], Olatunji Waliu Olademeji [a], Samson Oladayo Ayanlade [b], Etinosa Noma-Osaghae [b], Opeyemi Ahmed Ajibola [b]

[a] Department of Electronic and Electrical Engineering, Faculty of Engineering, Obafemi Awolowo University, Ile-Ife, 220103
[b] Department of Electrical and Electronics Engineering, Faculty of Engineering, Olabisi Onabanjo University, Ago Iwoye, 112104

ABSTRACT

This study developed a microcontroller-based system which coordinates and monitors hybrid renewable energy sources within a microgrid, providing an uninterrupted power solution for off-grid areas. Site data for wind speed, solar radiation, and load demand were collected and averaged into hourly intervals across seasons. A key novelty of this work is an intelligent coordination approach based on Sequential Quadratic Programming (SQP) that simultaneously determines economically viable system sizes and optimizes real time energy flow for adaptive, reliable, and cost-effective control. Mathematical models and size optimization were developed for all system components. This study proposes an intelligent coordination and optimal sizing framework for an off-grid hybrid renewable energy system comprising 500kW of solar PV, a 400-kW wind turbine, pumped hydro storage, battery–inverter units, and a biogas generator. The system is designed to supply the electricity demand of an academic facility using only renewable sources with biogas backup. Simulation results show that renewable energy meets up to 96.4% of the total load during weekends in June and 51.4% during weekdays in December, while storage units supply between 20.1% and 44.0% of the demand, thereby smoothing the variability of wind and solar resources. The proposed coordination strategy achieves a 70% reduction in fuel consumption and guarantees a reliable supply with a loss of power supply probability of zero, corresponding to a reliability level above 99%. Among the candidate configurations evaluated, the PV/wind/pumped hydro/battery/biogas system emerges as the most cost-effective, yielding a net present cost of 3.09M$ and a levelized cost of energy of 0.027$/kWh. These results demonstrate that the optimized hybrid configuration provides a techno-economically viable pathway for fully renewable, reliable power supply in remote institutional applications.

In conclusion, the study showed that implementing an off-grid HRES with sufficient storage can provide a sustainable solution for the electrification of remote areas not previously connected to the grid.

Keywords: Coordinating, Electrification, Monitoring, Microgrid, Microcontroller, Sustainable

1. Introduction

Nowadays, increasing power consumption drives the development of various forms of energy use worldwide. In Nigeria, grid extension remains the most popular electrification method. However, geographical isolation, dense jungles, rough landscapes, high costs, low-resource communities, low consumption, dispersed settlements, and poor roads often make grid connection impossible, [1]. Climate change effects from greenhouse gas emissions also push for less fossil fuel use. Energy crises, rising

Received 18 September 2025; revised 18 December 2025; accepted 23 December 2025.
Available online 19 January 2026

* Corresponding author.
E-mail addresses: babfisayo@gmail.com (O. S. Babalola), joseph.samson@oouagoiwoye.edu.ng (J. B. Samson), waliu2017@gmail.com (O. W. Olademeji), ayanlade.oladayo@oouagoiwoye.edu.ng (S. O. Ayanlade), ajibola.opeyemi@oouagoiwoye.edu.ng (O. A. Ajibola).

https://doi.org/10.70645/3078-3437.1053

oil prices, climate change from GHGs, and emission limits boost interest in efficient, eco-friendly technologies. Renewable energy systems are sustainable and nearly pollution-free, [2]. As a result, discovering new sources of energy to meet growing energy needs while reducing negative environmental effects is becoming an urgent task, [3, 4]. The energy crisis, rising oil prices, and climate change caused by GHG, and production limitations imposed on these gases have heightened people's interest in effective, efficient, and environmentally friendly technologies, [5]. Renewable energy systems that are both sustainable and almost pollution-free, [6]. The search for solutions that enhance the sustainability of current societal lifestyles is becoming more important to bridge the rapidly growing energy demand in emerging nations such as Nigeria. Since the hybrid renewable energy system combines different renewable energy sources, it is difficult for the system to be efficient and reliable without applying a proper control strategy.

This intelligent coordination refers to the system's ability to adaptively and optimally schedule energy dispatch by continuously updating inputs such as load demand and resource availability, ensuring reliable and cost-effective energy delivery through model-based supervisory control driven by SQP. The objectives of the control of a HRES are to monitor and coordinate the power flow of energy sources to satisfy the dynamic load demand.

Several researchers presented their views in different locations, and some are discussed as follows: [7] introduced a technique to examine an HRES comprising wind, solar, and battery components. It implements efficient control methods, including Maximum Power Point Tracking (MPPT) algorithms and Direct Power Control. Energy management strategies for optimal component interaction were developed, and the simulation studies validate these strategies under diverse conditions. However, the approach does not discuss the system's approach to managing unpredictable fluctuations in both renewable sources and load requirements, as well as Pumped Hydro Storage System dynamics. [8] developed a multi-agent system (MAS)-based intelligent energy management system for microgrids, focusing on decentralized control and agent coordination to manage distributed energy sources. The MAS framework improved system responsiveness and adaptability in a case study environment, enabling better load balancing and energy efficiency. However, the paper does not address how the system would handle stochastic variations in each renewable source and load demand, a key consideration for real-world microgrid reliability. [9] reviewed the use of artificial intelligence for optimizing renewable energy systems, highlighting techniques like machine learning, neural networks, and hybrid metaheuristics for forecasting, load prediction, and system efficiency. The paper emphasizes the role of AI in enhancing system reliability, reducing energy costs, and managing variability in renewable generation. However, it overlooked the gradual increase in energy demand resulting from population growth, and the considered algorithm proved to be inefficient for long-term, scalable integration in rapidly expanding energy systems. [10] proposed an intelligent forecasting and load management framework using a cascaded ANN and ANFIS to predict solar and wind power generation with high short-term accuracy. Tested on real-world data, the model demonstrated forecasting errors below 5%. Nevertheless, there was no mention of the system's control operation or scheduling in the face of stochastic variation in each renewable source and load demand, which limits its applicability in dynamic real-time environments. [11] developed a microcontroller-based intelligent hybrid energy control system using solar, wind, battery storage, and a diesel generator for off-grid applications. Simulations showed feasible performance across three energy penetration scenarios. Nothing was said about the system's control operation and scheduling in the face of stochastic variation in each renewable source and load demand, an essential aspect for ensuring uninterrupted power supply and system stability. [12] conducted a comprehensive review on grid modernization through the integration of renewable energy and intelligent technologies. The study covered AI applications, control strategies, and optimization algorithms like PSO and MPC, proposing a framework to guide grid transformation. While the review is broad and insightful, further research is needed to enhance the reliability and economically feasible integration of RES into the power system, especially under fluctuating supply and demand conditions. [13] developed a coordinated control for managing hybrid renewable systems, likely solar-wind-storage, to optimize energy flow and enhance power quality metrics like harmonics and voltage stability. It aligns with intelligent coordination for sustainable power supply through rule-based, relying instead on conventional control rather than nonlinear optimization for multi-objective HRES tasks. While effective for real-time management, it falls short of computational rigor for handling constraints in economic dispatch or Optimal Power Flow, limiting advanced sustainability features compared to SQP-based methods. [14] reviewed renewable energy integration challenges in power systems using a comprehensive literature analysis of control strategies, optimization algorithms, and storage solutions to address intermittency, grid

stability, and sustainability in hybrid renewable energy systems (HRES). The key contribution is a synthesized framework highlighting AI-driven forecasting and intelligent coordination for enhanced reliability and power quality, providing actionable pathways for sustainable power supply. However, it lacks in-depth coverage for nonlinear HRES optimization, leaving a gap in evaluating computationally efficient methods for constrained multi-objective coordination. [15] reviewed hybrid energy storage systems integrated with renewable power generation, focusing on configurations and control strategies to support reliable and efficient operation of hybrid renewable energy systems (HRES). The study covers combinations of batteries, supercapacitors, and flywheels with solar and wind sources, alongside intelligent control methods such as fuzzy logic and model predictive control for power smoothing and frequency regulation. While it highlights enhanced system reliability, cost efficiency, and lifespan extension, the review does not explicitly address optimization techniques related to intelligent coordination or sequential quadratic programming, which are critical for advanced control and management in sustainable HRES. It also points out ongoing challenges in standardized sizing and real-world scalability of hybrid storage systems. [16] reviewed decision-making, operational strategies, and coordination in energy storage systems with renewables, focusing broadly on performance optimization through indicators like efficiency and reliability. However, it does not explicitly address intelligent coordination or optimization techniques specific to hybrid renewable energy systems, such as sequential quadratic programming or advanced control schemes critical for sustainable hybrid energy management. The review also lacks emphasis on real-time and multi-objective optimization essential for resilient hybrid renewable power supply systems. [17] present a coordinated energy management system for a 4-wire 1-MW smart grid integrating three solar plants and three wind turbines to address power balancing, stability, and optimal utilization of hybrid renewable sources in real-time grid operations. Their hierarchical control scheme achieves seamless power sharing, voltage regulation, and reduced grid stress through coordinated renewable dispatch, demonstrating improved performance in simulations for sustainable supply resilience. The study primarily uses conventional rule-based and droop controls, which may limit the ability to handle economic dispatch, constraints, and uncertainties in more complex hybrid renewable energy system coordination. [18] review the impact of artificial intelligence on the planning and operation of distributed energy systems in smart grids, analyzing AI techniques like machine learning and neural networks to manage renewable integration challenges such as forecasting, optimization, and real-time control. The study evaluates AI applications in demand response, fault detection, and power flow optimization for enhanced grid reliability and efficiency with hybrid renewables. It demonstrates AI's role in reducing operational costs and improving stability but identifies gaps in computational scalability for large-scale systems and standardization of AI models across diverse grid infrastructures. [19] systematically review energy management controllers (EMCs), analyzing strategies, coordination mechanisms, architectures, and applications in microgrids and smart grids with renewables. The study categorizes EMCs into centralized, decentralized, and hybrid types, evaluating rule-based, optimization-based, and AI-driven approaches for power allocation and demand response. It demonstrates improved energy efficiency and grid stability through coordinated control but highlights gaps in real-time adaptability to uncertainties and scalability for large hybrid renewable systems. [20] reviewed smart grids for sustainable energy management, focusing on renewable integration, AI, and system challenges through systematic literature analysis. The methodology examines energy management systems, demand-side management, and AI techniques like Bayesian deep learning for load forecasting and grid optimization. It highlights coordinated approaches including energy storage, smart metering, and demand response, for improved reliability and efficiency in hybrid renewable systems. The review identifies gaps in cybersecurity and energy storage innovation requiring further development.

Recent studies on intelligent coordination of hybrid renewable energy systems (HRES) have employed reinforcement learning, fuzzy logic, and other AI-based control techniques to manage system uncertainty and nonlinear dynamics. Reinforcement learning methods offer adaptive decision-making capabilities but often require extensive training data and may suffer from convergence and constraint-handling challenges in practical power system applications. Fuzzy-logic-based approaches provide simplicity and robustness; however, their performance strongly depends on heuristic rule design, and they scale poorly for complex, high-dimensional coordination problems. Other AI-based controllers, such as neural networks, demonstrate strong nonlinear modeling ability but typically lack transparency and explicit constraint enforcement. In contrast, the proposed intelligent coordination approach emphasizes reliable convergence and deterministic constraint satisfaction while maintaining competitive economic and operational

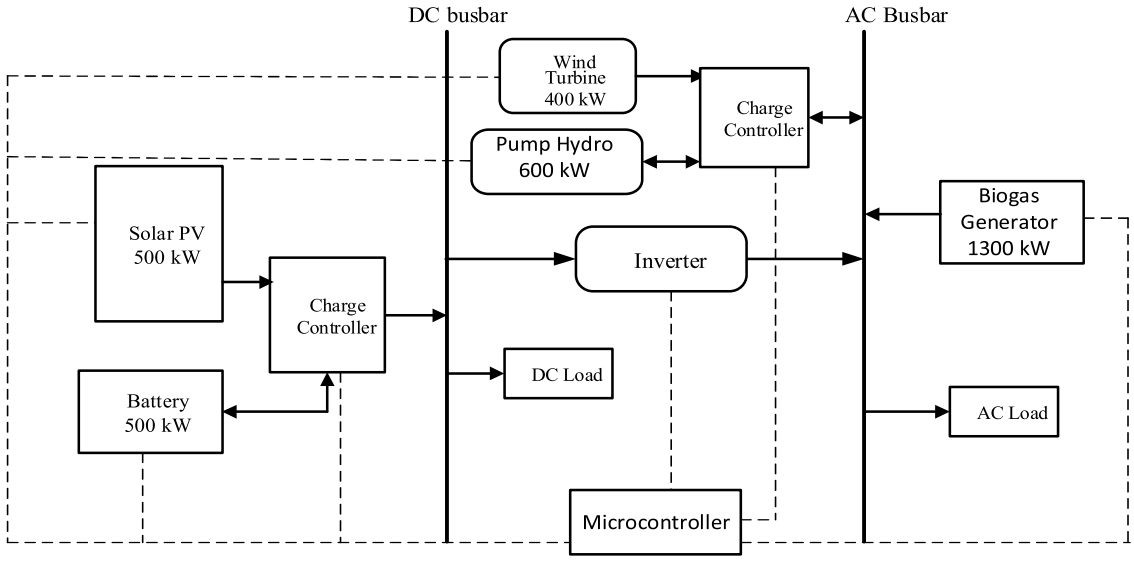

Fig. 2.1. Implementation strategy for a hybrid power system.

performance, making it well-suited for sustainable and practical HRES deployment. To overcome these challenges, this study adopts Sequential Quadratic Programming (SQP), a robust optimization method well-suited for nonlinear problems with constraints, offering a practical balance between computational efficiency and real-time adaptability. In addition, the research develops an advanced control system integrating multiple storage technologies and biogas to enhance system resilience against component failures and extreme weather dynamics. This approach aims to increase renewable energy participation in load sharing while reducing dependence on biogas, ultimately delivering a cost-effective and reliable off-grid hybrid renewable energy system.

The proposed hybrid system—comprising photovoltaic panels, wind turbines, pumped hydro storage, batteries, and a biogas generator designed to supply electricity to the academic campus of Obafemi Awolowo University, demonstrates the practical relevance and scalability of the solution. In summary, this paper presents a microcontroller-based coordination system for off-grid hybrid renewable energy supply, leveraging SQP for real-time energy optimization. The proposed method improves energy efficiency and reliability through dynamic source coordination and storage integration. The subsequent sections of this paper are structured as follows: The methods used for carrying out this study, which include mathematical modeling and computer programs for simulations were described in Section Three. Section Four gives the results and discussion of the simulation of the developed algorithm. Finally, Section Five provides the conclusion of the work and recommendations based on the research findings.

2. Methodology

2.1. The hybrid power system model

As shown in Fig. 2.1, the HRES comprises PV panels (500 kW) and a deep cycle battery (500 kW) connected to the DC busbar via a charge controller, providing a low-voltage load supply. The AC busbar hosts the wind turbine (400 kW), pumped-hydro storage unit (600 kW), and a biogas-fueled generator (500 kW) as a backup source. An inverter allows bidirectional power flow between the AC and DC busbars, ensuring seamless energy utilization across load demands.

The microcontroller monitors generation levels, load requirements, and storage status, making dispatch decisions based on a hierarchical control algorithm. The microcontroller prioritizes direct utilization of PV and wind generation, charging the storage units when surplus occurs. When load demand exceeds generation, the controller sequentially discharges the battery and pumped-hydro storage. The biogas generator is activated only when necessary, preserving fuel and minimizing emissions. This architecture and control scheme enable an optimized, robust, and resilient solution for off-grid or remote electrification. Additionally, a microcontroller continuously monitors and coordinates power flow to ensure optimal operation and seamless integration of all energy sources, ensuring a reliable and sustainable

solution for electrification in off-grid or remote areas.

The wind speed data and load demand data, along with solar photovoltaic (solar PV) radiation, were collected from Obafemi Awolowo University's main campus for this study. The objective was to determine component size and develop an effective off-grid HRES operational model for the university community. The system's focus is to limit the biogas-generating set's operation and minimize charging-discharging cycles of the battery. To achieve this, a robust scheduling of renewable sources was implemented, ensuring the biogas generator only operates during renewable source insufficiency. The research followed a structured order, beginning with resource assessment, where wind speed and solar PV irradiance data from 2016 to 2019 were obtained. Next, the demand assessment involved processing load demand data for various scenarios. Components sizing were performed using the Sequential Quadratic Programming method, leading to the design of an integrated HRES with appropriate RES sizes. An algorithm was developed on MATLAB/Simulink to coordinate the HRES, and the system's performance was evaluated by analyzing the RES' contribution ratio.

The MATLAB simulation was conducted over a 24-hour scheduling period with a timestep of 1 hour, corresponding to the resolution of the input data. The 1-hour average data was used directly at each timestep without interpolation. Inverter efficiency of 90% was incorporated to reflect real operating conditions. Data preprocessing steps such as outlier removal and smoothing were applied to improve data quality. These details enhance the reproducibility and accuracy of the simulation.

2.2. System coordination strategy

[21] supervisory control system was modified to include a PHSS and a biogas generator. The control algorithm used in this study is based on Sequential Quadratic Programming (SQP), a nonlinear optimization technique that coordinates power flow among hybrid renewable energy sources. At each time step, the algorithm receives input data including load demand, available wind and solar power, battery state of charge (SoC), and storage system status. It formulates an objective function that minimizes the overall energy cost while meeting constraints such as energy balance, source capacity limits, and storage SoC boundaries. The SQP solver computes the optimal power contribution from each source—solar PV, wind, battery, biogas, and pumped-hydro—ensuring that the total generation meets the load demand reliably. The calculated outputs are sent to the microcontroller, which activates the appropriate switches to dispatch energy from each source. This coordination process is repeated continuously to adapt to changing resource availability and demand profiles. This increases RE participation in the load sharing, while reducing the need for biogas. In the process of developing the algorithm for the coordination of this HRES, the following suppositions were made:

i. The system's components are considered to have the following order of priority as related to their dispatch: solar PV - wind – energy storage devices (pumped-hydro and battery) – biogas generator.
ii. Each source (solar PV, wind, biogas, battery, pumped hydro) is assumed to operate within its rated capacity, and power output is constrained by real-time availability (e.g., solar irradiance and wind speed).
iii. Power transmission between components is assumed to be lossless and instantaneous. This simplifies the real-time coordination logic and focuses on generation and storage optimization.
iv. If the total power generated by either or a combination of the RES is greater than the load demand at a particular time, the energy surplus is stored in the storage devices until the devices reach the maximum capacity.
v. If the total power generated by the RES is less than the load demand, the energy deficit is covered by the storage devices, if the energy levels of the storage devices are adequate. The battery will take up immediately while the pumped-hydro gathers momentum. If the output from the PHSS is sufficient, the battery will be disconnected.
vi. If the load demand should exceed the capacity of the total generation of renewable sources and the storage devices, the biogas generator is switched on to supply the deficit. This will usually occur at peak periods and worst climatic conditions.

2.3. System sizing for renewable energy systems

The optimal size of each component was determined to ensure an economical and reliable hybrid energy system. If the components are undersized, the reliability of the hybrid energy system would not be guaranteed. Also, if any of the components is oversized, the system may be economically unsatisfactory. In this study, the main economic parameter for sizing components is the generation cost of electricity per kW. The Levelized Cost of Electricity (LCOE) is obtained from the total cost per kW of each RES,

and it is used to measure the economic viability of RESs. The LCOE of any RE project is determined by its total capital costs, resource quality/potential, technical characteristics of the conversion system, operation and maintenance costs (O & M), economic lifetime of the project, technical year of usage, and discounted rate (in per cent) IRENA, (2021). The simplified model of the LCOE, [22] was used in this study, as given by Eq. (2.1).

$$LCOE = \frac{C_k + \sum_{t=1}^{n} \frac{R_k}{(1+d)^t}}{\sum_{t=1}^{n} \frac{E}{(1+d)^t}} = \frac{\left(K_w P_w + K_{PV} P_{PV} + K_{bgen} P_{bgen} + C_f\left(P_b\right)\right)}{E} \quad (2.1)$$

Where C_k is total capital costs, R_k is (O & M) costs, n is economic lifetime of the project, t is lifetime of usage, $d$is discount rate (in percent). In Eq. (2.1), the numerator is the net total cost, which comprises both the capital investment and the operational costs of the renewable system. The denominator is the total electrical energy produced by the system, in kWh. The aim of the study is to present a cost-effective off-grid HRES.

The optimization process, which is built into simulations with objective functions to minimize net present cost and LCOE, computes the number of wind turbines, optimal size of the PV array, number of batteries, and size of the inverter to ensure that residential load demand is met all the time. Hence, the optimization problem to be solved involves the minimization of the net present cost (NPC) under the constraints of providing the load with power balance and system limits and satisfying the constraint of sustainability as shown in Eqs. (2.2) to (2.6):

$$\text{Minimize} \quad \left(C_k + \sum_{n=1}^{n} \frac{R_k}{(1+i)^t}\right) = \left(K_w P_w + K_s P_s + K_{bgen} P_{bgen} + C_f\left(P_b\right)\right) \quad (2.2)$$

$$\text{Subject to} \quad P_w + P_s \geq P_{load(ave)} \quad (2.3)$$

$$\left(P_w + P_s + P_{bgen}\right) = P_{load(\max)} \quad (2.4)$$

$$P_{bgen}{}^{\min} \leq P_{bgen} \leq P_{bgen}{}^{\max} \quad (2.5)$$

Where

$$C_f\left(P_{bgen}\right) = f_0 + f_1 P_{bgen} + f_2 \left(P_{bgen}\right)^2 \quad (2.6)$$

K_w, K_s and K_{bgen} are the electricity costs per kW for wind turbines, solar PV, and biogas, respectively. P_w, P_s and P_{bgen} are of each system, respectively, C_f is the equation for the fuel gas consumption cost of biogas generators and f_0, f_1 and f_2 are the fuel consumption coefficients. Since the objective function is a non–linear function that is twice differentiable, it satisfies the conditions for convexity; As a result, the quadratic programming approach can be used to solve the minimization problem.

The algorithm in MATLAB was used to solve the SQP problem in this work. Table 2.1 shows the selected parameters. The maximum and average load demand for the busiest day (DAY 1) was used for the constraints. A biogas-fueled generator was used in this study due to its environmentally friendly recirculation of organic waste. Whenever the load demand is less than the generated power from the renewable systems, the surplus energy will be adequately stored in the incorporated storage devices, and when the load is more than the generated power from the renewable systems, the deficit is taken from the storage devices or the biogas, as the case may be. The flowchart for the optimization procedure is shown in Fig. 2.2. Based on the outcome of the optimization results, specifications for the wind and PV systems, and the other components (storage devices, backup biogas) are determined.

2.4. Mathematical models for system's components

The meteorological and load demand data for the area under consideration; and the results of the optimization process were used to estimate the specifications of all the components that constitute the HRES. The coordination strategy of the integrated RES was developed based on these specifications.

2.4.1. The wind system

From the result of the optimization, the size of the wind energy system was obtained to give a rated

Table 2.1. Parameters for optimal sizing of the system's components.

Components	Cost ($/kW)
Wind	1,500
Solar PV	2,500
Pumped hydro	350
Battery	450
Inverter	140
Biogas	470
Fuel co-efficient (Biogas power) at $ 0.65 per m^3/kWh	
f_0($)	8.57
f_1($/kW)	4.76
f_2($/kW^2)	0.15
Load demand values for weekdays in the academic session	
$P_{load(ave)}$	1.2 MW
$P_{load(\max)}$	0.8 MW

Sources: [23]; IRENA 2021 + NREL ATB 2023; NREL 2020).

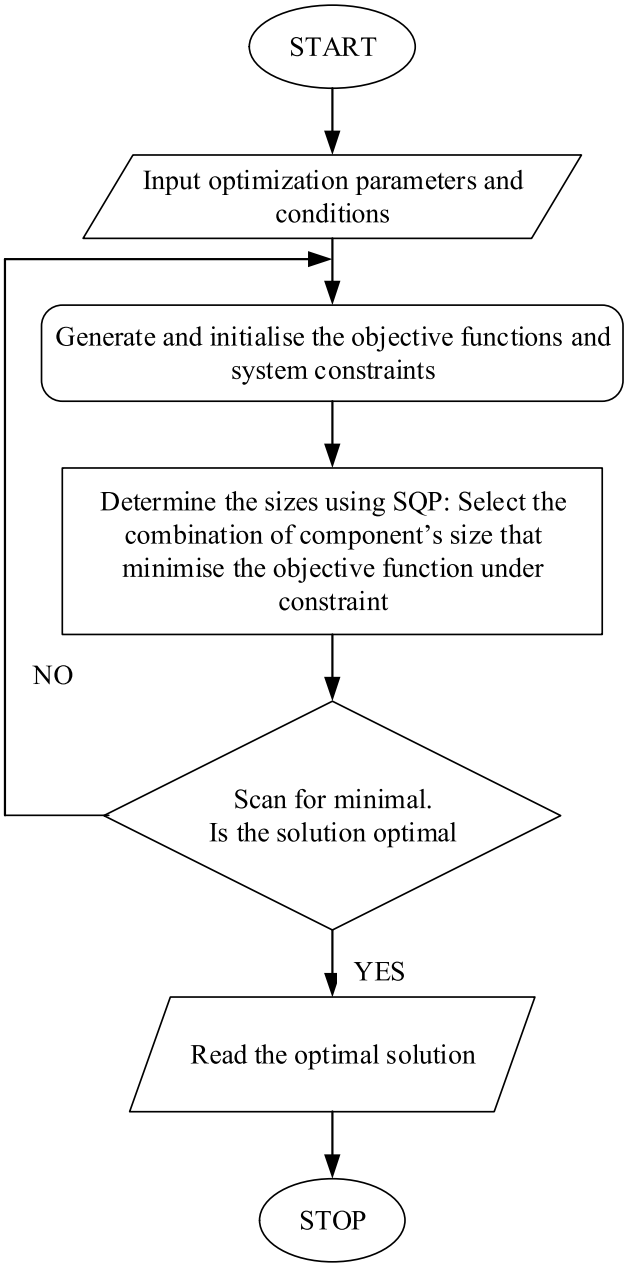

Fig. 2.2. Flowchart for determining the appropriate component size.

power capacity, P_{wrated}= 400 kW. The wind energy system's electrical instantaneous power is expressed by Eq. (2.7):

$$P_w = \frac{1}{2}(\eta_w \times \eta_g \times C_{p,\max} \times \rho_a \times A \times {v_w}^3) \quad (2.7)$$

Where P_w = wind turbine electrical power (MW), η_w: The mechanical (gearbox) (%), η_g = Electrical generator efficiency (%), ρ_a = Air flow density (kg/m^3), v_w = Wind speed (m/s),A = Rotor swept area (m^2), [24]. The coefficient of the wind turbine Power is a measure of how effectively the turbine converts kinetic energy in the wind into electricity. It depends on the tip speed ratio as well as the blade pitch angle, β. The practical power coefficient of the wind energy conversion system is given by Eq. (2.8):

$$C_p(\lambda, \beta) = \eta_w \times \eta_g \times C_{p,\max} = 0.75 \times C_{p,\max} = 0.449 \quad (2.8)$$

The maximum power coefficient, $C_{p,\max}$ is technically called the Betz limit; and $C_{p,\max} = 0.599$.

In this study, an Enercon 400 kW wind turbine model that has a rated wind speed, $v_{w,t}$= 8.5 m/s, was used. For an onshore wind energy system with a rotor diameter of 59.0 m, blade swept area is A = 2,735 m^2. The hub (tower) height is taken to be 40m above ground level and the density of air (onshore) is taken to be $\rho_a = 1.25$ kg/m^3. Hence, Eq. (2.7) yields

The wind generator's actual output as a function of instantaneous wind speed is:

$$P_{w\max} = \frac{767.5 \times (v_w)^3}{1000} = \frac{767.5 \times 8.05^3}{1000} = 400.4 \text{ kW} \quad (2.9)$$

Where, v_{ci} is the cut in wind speed, v_{co} is the cut-out wind speed, v_r is the rated wind speed, $v_{w,t}$ is the wind speed at a particular time and P_{wrated} is the rated power of the wind energy system.

The tower should be tall enough to raise the turbine above the air turbulence close to the ground and the bottom edge (tip) of each turbine blade should be at least 10 m above any obstacle within 150m of its location. The suitable site for the wind energy system is elevated land such as the hill. The wind system, considered in this study, is designed for high reliability, low maintenance and moderate wind sites.

2.4.2. The solar photovoltaic system

From the result of the optimization, the solar PV system was sized to give a maximum rated power of, P_{srated} = 500 kW. The solar PV panel adopted in this study is the monocrystalline type because of its high efficiency rating and high-power output yield. The output power of each PV panel is calculated from the relation:

$$P_s = \eta_{pv} \times N_{pvp} \times N_{pvs} \times V_{oc} \times I_{sc} \text{ (W)} \quad (2.10)$$

P_s is the total power output of the solar array, η_{pv} is the efficiency of the photovoltaic module, N_{pvp} is the number of PV panels connected in parallel, N_{pvs} is the number of PV panels connected in series, V_{oc} is the open-circuit voltage of a single PV panel, I_{sc} is the short-circuit current of a single PV panel, [25].

The standard and commercially available PV panels have an implementable efficiency value of approximately 23.1 percent. Each solar PV panel comprises of parallel connection of 6 strings of PV cells and each string is made up of 36 PV cells connected in series ($\eta_{pv} = 0.231$, $N_{pvs} = 36$, $N_{pvp} = 6$). V_{oc} and I_{sc} are the solar panel's open circuit voltage and short-circuit current respectively, at a standard simulation temperature of 25 °C.

The solar photovoltaic panel's generates electrical power, as a function of instantaneous irradiation value, G_t is given by Eq. (2.11):

$$P_{pv}(G_t) = \begin{cases} P_{srated} \times \frac{G_t^2}{G_{std} R_c} & 0 \le G_t < R_c \\ P_{srated} \times \frac{G_t}{G_{std}} & G_t \ge R_c \end{cases} \quad t = 1, 2, \ldots, T \tag{2.11}$$

Where G_{std} is the solar radiation in the standard environment set as 1000W/m^2, R_c is the threshold radiation point set as 150 W/m^2 and P_{srated} is the equivalent rated power output of each solar PV panel ($P_{srated} = 350$ W), $Gt$is the Solar irradiance (kW/m^2), [25].

2.4.3. Pumped hydro storage system

The main storage in this design is the pumped-hydro which consists of variable speed pump-as-turbine (PAT) system. The introduction of PHSS is based on the following assumptions:

a. The power available for storage in the PHSS arises from the surplus power from the wind system.
b. The maximum energy capacity of the PHSS should be able to generate, $P_{hrated} = 400$ kW over a 24-hour period, $T_{\max}$:

$$E_{l,\max} = P_{hrated} \times T_{\max} = 9.6 \text{ MWh} \tag{2.12}$$

$$E_{l,\min} = P_{hrated} \times T_{\min} = 0.4 \text{ MWh} \tag{2.13}$$

The maximum and minimum energy holding capacity ($E_{h,\max}$ and $E_{h,\min}$) of the pumped-hydro reservoir were estimated from the maximum and minimum load energy requirements from the PHS in MWh as shown:

For a day (maximum):

$$E_{h,\max} = \frac{E_{l,\max}}{\eta_h} = 12.8 \text{ MWh} \tag{2.14}$$

For a one-hour period (minimum):

$$E_{h,\min} = \frac{E_{l,\min}}{\eta_h} = 0.53 \text{ MWh} \tag{2.15}$$

η_h is the efficiency of pumped-hydro storage being 75% in both generation and pumping modes from Table 2.2. The (PPHS) can be in either pumping mode or generation mode at any instance of time, depending on the amount of load consumption and the instantaneous power by the wind system.

The amount of stored energy in the pumped-hydro storage at any time (pumping mode) can be calculated from the wind system as follows.:

$$E_h^+(t) = \sum^{N_t} \eta_h (P_w(t) - P_{load}(t)) T; \quad \text{for} \quad P_w(t) > P_{load}(t) \tag{2.16}$$

$$E_h^+(t) = \sum^{N_t} (\eta_h P_w(t)) T; \quad \text{for} \quad P_w(t) < P_{load}(t) \tag{2.17}$$

$$E_h^+(t) = 0; \quad \text{for} \quad P_w(t) = P_{load}(t) \tag{2.18}$$

$E_h^+(t)$: The accumulated energy stored in the hydro storage system at time t, N_t is the time interval (number of time steps) when the device is active (pumping) and the relevant time step, T = 1 hour, η_h: The efficiency of the hydro pump system, $P_w(t)$: The power available from the wind turbine at time t, $P_{load}(t)$: the amount of power required by consumers

The total energy after pumping is given as:

$$E_h(t) = E_h(t-1) + E_h^+(t) \tag{2.19}$$

Eq. (2.20) can be used to calculate the energy output required from pumped-hydro storage at any time (generation mode):

$$E_h^-(t) = \frac{\sum^{N_t} (P_{load}(t))^T}{\eta_h} \tag{2.20}$$

N_t represents the interval (in number of time steps) during which the device operates in generation mode, where each time step has a duration of T = 1 hour. The total energy remaining after generation is:

$$E_h(t) = E_h(t-1) - E_h^-(t) \tag{2.21}$$

Given the hydraulic head, H; an upper bound on flow rate, q and the efficiency of the device, $P_h^g =$ Stored hydro energy, $\rho =$ Density of water (typically 1000 kg/m^3), $g =$ Acceleration due to gravity (9.81 m/s^2), $H =$ Height difference between reservoirs (m), η_h, the power generated in generation mode and the power consumed in the pumping mode, in one hour,

Table 2.2. Characteristics of Common Types of Energy Storage Sources.

Type	Output Power (MW)	Energy Capacity (MWh)	Energy Density (Wh/kg)	Power Density (W/kg)	Efficiency (%)	Response time (s)	Life (year, y; cycle, c)
Pumped hydro	0–1800	>200	0.5–1.5	-	75	10–600	50y
Compressed Air	0–300	0–105	30–60	10–100	64	1–600	30y
Superconducting Magnetic Energy Storage	0–10	0–1	30–100	10^4–10^5	95	0.005	30y
Fly wheel	0–5	0–10	10-May	10^2–10^3	93	0.05	20y
Super capacitor	0–0.3	0–10	<50	0–4000	98	0.05	10^5c
Battery	0–50	0–100	30–200	0–500	70–80	0.02	3000c

(year, y; cycle, c) Source: [26].

by the pumped-hydro storage can be calculated according to the Eqs. (2.22) and (2.23), respectively, [24]:

$$P_h^g = \eta_h \times \rho \times g \times q \times H \tag{2.22}$$

$$P_h^p = \frac{\rho \times g \times q \times H}{\eta_h} \tag{2.23}$$

2.4.4. Batteries

Any surplus energy from the solar PV array will be diverted to charge the battery. As a result, the energy storage capacity of the battery, if all the energy from the PV system in a day is to be stored, is estimated from Eq. (2.24):

$$E_{PV} = T \times \sum_{n=1}^{N_t} P_{PV}(t) \tag{2.24}$$

N_t is the time interval (number of time steps) during which the solar PV panel is generating electricity and each time step, T = 1 hour. For this study, the energy storage capacity will be determined by the average energy output of the solar PV system in a day (in MWh). Hence, using an estimated average solar PV availability of about 5.8 hours per day for southwest region of Nigeria, the average daily energy from PV system, with $P_{PVrated} = 500$ kW, was estimated as given by Eq. (2.25).

$$E_{PV,ave} = \frac{P_{PVrated} \times t_{ave}}{1000} = \frac{500 \times 5.8}{1000} = 2.9 \text{ MWh} \tag{2.25}$$

Hence, the maximum state of charge of the battery was estimated from the possible average daily solar PV energy as:

$$E_{b,\max} = \frac{E_{s,ave}}{\eta_b \times \eta_i} = \frac{2.9}{0.78 \times 0.90} = 4.1 \text{ MWh} \tag{2.26}$$

The efficiencies of battery, $\eta_b = 78\%$ (during charging only) and Inverter, $\eta_i = 90\%$ (for both charging and discharging mode).

The depth of discharge, $DoD = 80\%$. Hence, the battery's minimum state of charge was calculated as:

$$E_{b,\min} = SoC_{\min} = 0.2 \times 4.1 = 0.82 \text{ MWh} \tag{2.27}$$

Due to the energy holding capacity (charging depth) of the battery, there is a limit to how much energy the battery can be charged by excess renewable energy. This determines the maximum duration of charging (*DoC*), the state of charge (*SoC*) and the depth of discharge (*DoD*) of the battery.

At charging mode, the energy supplied to the battery through the charge controller at any given time is calculated from the solar PV system as:

$$E_b^+ = \sum^{N_t} \eta_b \left(P_{PV}(t) - \frac{P_{load}(t)}{\eta_i} \right) T; \quad \text{for} \quad P_{PV}(t) > P_{load}(t) \tag{2.28}$$

$$E_b^+(t) = \sum^{N_t} (\eta_b P_{PV}(t))\, T; \quad \text{for} \quad P_{PV}(t) < P_{load}(t) \tag{2.29}$$

$$E_b^+(t) = 0; \quad \text{for} \quad P_w(t) > P_{load}(t) \tag{2.30}$$

E_b^+ = battery charging mode, $P_{PV}(t)$ = rated PV power, $P_{load}(t)$ = load, η = efficiency of the battery, N_t is the time interval (number of time steps) during which the battery charges, the time step, T = 1 hour, and σ is the self-discharging factor of the battery. The total battery energy at time t, after charging is given as:

$$E_b(t) = (1 - \sigma) \times E_b(t-1) + E_b^+(t) \tag{2.31}$$

At discharging mode, at any given time, the energy output from the battery through the inverter and

charge controller is estimated as:

$$E_b^+(t) = \frac{\sum^{N_t} (P_{load}(t) - P_b(t))\, T}{\eta_i} \quad (2.32)$$

N_t is the time interval (number of time steps) during which the battery discharges, the time step, T = 1 hour and σ is the self-discharging factor of the battery. The total battery energy at time t, after discharging is given as:

$$E_b(t) = (1-\sigma) \times E_b(t-1) - E_b^-(t) \quad (2.33)$$

The efficiency of the battery is taken to be η_b = 78%. Hence, the battery absorbs (charges) at 78% efficiency from Table 2.2, and it delivers (discharges) at 100% efficiency, [25]. Deep cycle batteries are recommended for use in solar PV systems. Deep cycle batteries are designed to be discharged to a low energy level and then rapidly recharged (charging and discharging cycles) day after day for an average of 3000 cycles.

As mentioned earlier, the battery is meant to store the unused energy from the PV system and to be used alongside the pumped-hydro storage, so using the maximum daily load requirement for the determination of battery size may lead to an excessively sized battery bank. Hence, the ideal minimum size of the battery bank for one day of autonomy was estimated by using the average daily energy that the solar PV system generates, as shown:

$$C_b = \frac{E_{PV,ave} \times S_{days}}{\eta_b \times \eta_i \times DoD \times V_{bat}} \quad (2.34)$$

Using $E_{PV,ave}$ from Eq. (2.35),

$$C_b = \frac{2.9 \times 10^6}{0.78 \times 0.9 \times 0.8 \times 12} = 4.3 \times 10^5 \text{ Ah} \quad (2.35)$$

2.4.5. Biogas

Most biogas generators are not allowed to run at less than 30% of their rated power. Thus, in this study, the limits are chosen as $P_{Bgen}^{(\min)}$ = 30% and $P_{Bgen}^{(\max)}$ = 95% of rated power. Hence, the rated power of the generator, $P_{Bgen}^{(rated)}$ = 1300 kW; and the generator's output's minimum and maximum limits are $P_{Bgen}^{(\min)}$ = 390 kW and $P_{Bgen}^{(\max)}$ = 1235 kW respectively.

The power output limit of the biogas is a significant constraint that was modeled into the system. The biogas generating unit's real power output is restricted between the upper and lower limits as shown in Eq. (2.36).

$$P_{Bgen}^{(\min)} \le P_{Bgen(t)} \le P_{Bgen}^{(\max)} \quad (2.36)$$

$P_{Bgen}^{(\min)}$ = biogas generating at the lower limit, $P_{Bgen}^{(\max)}$ = biogas generating at the upper limit, [24].

1. Algorithm for the microcontroller system on MATLAB

The algorithm performs optimal power flow (OPF) in the hybrid renewable energy system (HRES) using a Sequential Quadratic Programming (SQP) approach. The optimization objective is to minimize the Levelized Cost of Energy (LCOE) of the system over its operational lifespan. This economic metric captures both capital investment and ongoing operational costs, providing a cost-effective basis for comparing energy mixes. Optimization is subject to several constraints, including power balance (i.e., matching generation and load in real time), system operational limits (such as generator and storage capacities), and sustainability targets (such as maximizing renewable energy usage and minimizing biogas fuel consumption).

SQP was chosen for its ability to handle nonlinear, constrained problems involving continuous variables, making it well-suited to the multi-source nature of HRES. Compared to simpler rule-based dispatch algorithms or heuristic methods (e.g., PSO, GA), this approach enables a more mathematically rigorous and economically optimal dispatch strategy. While recent studies have explored metaheuristics and deep reinforcement learning (DRL) for OPF in microgrids [e.g., [27, 28], SQP-based method offers a reliable and computationally efficient alternative for embedded system implementation, especially where system models and constraints are explicitly defined.

A microcontroller acts as the central intelligence that efficiently manages and coordinates HRES components. It senses data from the system and executes advanced control algorithms to optimize operations. It dynamically balances energy flow to meet demand and maximize system efficiency. Each renewable energy device and other component can be monitored and controlled via an interface into the microcontroller and the system seamlessly interfaces into the remote management database, providing reports on renewable energy usage and other system conditions. The operational procedures of the microcontroller system that guide the scheduling of the HRES were detailed in the flow chart shown in Fig. 2.3

During the storage mode, either or both renewable energy systems are generating more than the load requirements. If the power generated from each of the systems exceeds the load requirements, the wind

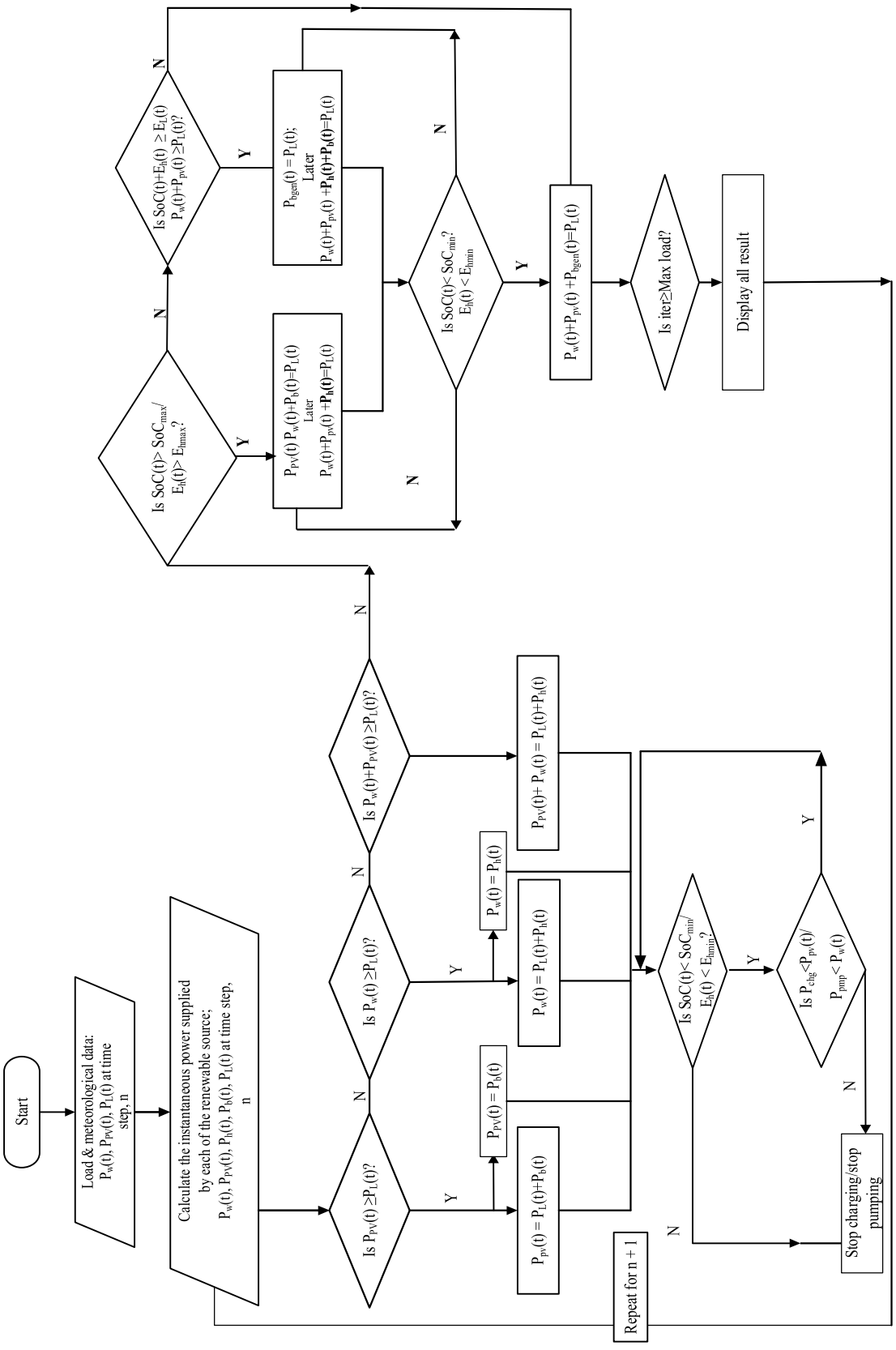

Fig. 2.3. Flowchart for the system's coordination.

energy system supplies the load power, while the excess wind power and the whole power from the solar PV energy system pump water into the PHSS and charge the battery, respectively. If the wind system's power is insufficient, the solar PV system is checked; and if the solar PV power is sufficient, solar PV energy system supplies the load power, while the excess power from the solar PV system and the wind energy system charges the battery and pump water into the PHSS, respectively. If the power generated by each of the energy systems is less than the load demand, their combination will be used. In this case, the excess energy from the combined renewable energy systems, after the load has been met, will be used to pump water into the PHSS. The storage systems enter usage mode when the combined output of the two renewable sources cannot meet the load.

The contents of the storage devices will be checked, if both storage devices have sufficient energy content such that the minimum permissible energy level will not be violated, the deficit will be taken from the storage facilities, with the battery responding faster than the PHSS. Otherwise, the biogas will be used to supply the deficit. The equation estimates the total power in the HRES at each time step (2.37):

$$P_{hybrid}(t) = P_{load}(t) + P_{loss}(t) = P_w(t) + P_s(t) + P_{sto}(t) + P_{gen} \quad (2.37)$$

$$P_{sto}(t) = P_h(t) + P_b(t) \quad (2.38)$$

where $P_{sto}(t)$ is the total contribution from both storage facilities and $P_{loss}(t)$ is the power loss.

2.5. Collection and processing of results

For accessibility of results needed for evaluating the performance of the developed algorithm under different weather and load conditions, a graphical user interface (GUI) for the microcontroller was developed. The interface consists of the input panel and the result panel. The input panel has four columns namely: Time step, Load demand, Wind speed (m/s), and Solar PV radiation (W/m^2) (MW). The output/result panel consists of the following: Load demand, (MW), Wind power, (MW), Solar PV power, (MW), Pumped-hydro energy state (MWh), Pumped hydro power, (MW), Pumped-hydro mode, Battery energy state (MWh), Battery power, (MW), Battery mode, Biogas Generator power, (MW), Biogas Generator mode, and Service systems, respectively.

The column for service systems displays the code(s) of the energy system(s) that are in generation mode at a particular time step. The following codes are allotted to each system: 1 – Solar PV system, 2 – Wind system, 3 – Pumped-hydro storage, 4 – Battery storage and 5 – Biogas, and the mode of each of the energy storage systems and biogas is as described under Section 2.2. The wind and PV power recorded at each interval is the total generated power from the systems at that time.

As a result, the total power available from renewable energy systems (wind and PV) within the HRES at any given time was estimated using Eq. (2.39):

$$P'_{ren}(t) = P_w(t) + P_{PV}(t) \quad (2.39)$$

The actual input of RES (with storage) satisfying the load estimation was performed using Eq. (2.40).

$$P_{ren}(t) = P'_{ren}(t) + (P_h(t) + P_b(t)) = P_{load}(t) - P_{gen}(t) \quad (2.40)$$

Where $P_w(t)$, $P_{PV}(t)$, $P_h(t)$, $P_b(t)$ and $P_{gen}(t)$ are the wind's instantaneous power, PV, pumped-hydro, battery, and the biogas, respectively. $P_{load}(t)$ is the load demand at any given time, t.

2.6. Properties of each control unit

The following properties and discrete values were assigned to the storage and biogas component of the hybrid system at different modes of operation:

i.	Pump-hydro System Possible modes of operation:	Pumped-hydro –	Pump Generator Standby	'–1' '1' '0'
ii.	Battery system Possible modes of operation:	Battery -	Charging Discharging Standby	'–1' '1' '0'
iii.	Biogas generator Possible modes of operation:	Biogas -	Generation Standby	'1' '0'

2.7. Cost analysis

Finance is an important factor that impacts the feasibility of a project. A few economic inputs, such as total capital cost, interest rates, and project duration, influence this. The NPC and the LCOE are the main indicators utilized to categorize the best system's results. NPC includes all costs incurred during the project's lifetime, such as the initial capital cost, (O & M) costs, and replacement costs. This value includes all revenues, including salvage values for system components, that have been deducted over the project's lifetime. The NPC for the study is calculated

using Eq. (2.41), [29]

$$NPC = \frac{C_{ann.total}}{CRF\,(i,n)} \tag{2.41}$$

where capital recovery factor (CRF) is given as:

$$CRF\,(i,n) = \frac{i(1+i)^n}{(1+i)^n - 1} \tag{2.42}$$

where $CRF_{ann.total}$ is the total annualized cost, n is the number of years, and i is the annual interest rate calculated as [29]

$$i = \frac{i' - f}{1+f} \tag{2.43}$$

LCOE is the cost per unit of electricity generated by the hybrid system. This is calculated as:

$$LCOE = \frac{C_{ann.total}}{E_{served}} \tag{2.44}$$

where E_{served} is the total electricity load served by the system.

3. Results and discussion

3.1. Introduction

The results of the simulation of the designed HRES are presented in this chapter. Microsoft Excel was used for data processing before simulation, while MATLAB/Simulink R2021a was used for simulations.

3.2. Optimal sizes of the system's components

The optimization algorithm (Section 3.4) for sizing the HRES components was written in MATLAB code. The optimization process yielded optimal power ratings of 400 kW, 500 kW, and 500 kW for wind systems, solar PV, and a biogas generator. At these values, the system's net capital cost is minimal. However, the biogas generator rating was chosen to be sufficient to supply the maximum load demand. This is done to facilitate all-around reliability and availability during the period of maintenance (servicing, overhauling, and replacing) and during the time of insufficiency of renewable energy, due to changing meteorological conditions. The power ratings of the wind energy system and photovoltaic system were chosen to be 400 kW and 500 kW, respectively, based on the result of the optimization procedure.

The results of the optimization process gave the optimal size of both the wind and solar systems to be 400 kW, while the optimal size of the biogas generator was obtained as 500 kW. However, due to the uncertainty surrounding the availability of the two renewable systems (as a result of fluctuations in climatic conditions), the backup biogas generator was sized to be 1300 kW. This ensured that the maximum load demand of the studied site can be met with only a biogas generator if the hybrid energy system experiences very bad climatic conditions. The (PPHS) and the battery were sized based on the power ratings of the wind and solar energy systems, respectively. Another factor that governed the sizing of the storage devices is their cost per kW, which is high for battery storage when compared to the PHS.

3.3. Performance analysis and evaluation of a hybrid renewable system

The results obtained from the simulation for the optimal output power coordination of the HRS are presented in Table 3.1 to Table 3.10. Based on these results, further analyses that explain the objectives of this work were carried out and presented in subsequent sections. The screenshot of the microcontroller is shown in Fig. 3.1.

This microcontroller-based, cost-effective, and flexible design is successfully implemented in MATLAB. and it showed acceptable results in meeting the load demand.

In Table 3.11, eight of the ten scenarios show that RESs play a significant role in satisfying the load demand of the site being studied over the 24-hour scheduling horizon. For six of the five load conditions considered, (c), (d), (e), (h), (i) and (j) of both Sundays in the rainy (June) and dry season (December) show a remarkable contribution of 81.3%, 96.4%, 71.4%, 81.1% and 91.2%, respectively, to satisfying the load demand of the site being studied.

The biogas generator's contribution to load supply is greatly reduced, as shown in Fig. 3.2c, Fig. 3.2d, Fig. 3.2e, Fig. 3.3h, Fig. 3.3i, and Fig. 3.3j with a contribution of 30.9%, 18.7%, 3.59%, 28.6%, 18.6% and 8.76% respectively. The rain (June) and dry season (December) also demonstrate a substantial potential for generating RE of about 44.3%, 44.1%, 53.0% and 51.4% for four out of the five load conditions, as shown in Fig. 3.2a, Fig. 3.2b, Fig. 3.3f, and Fig. 3.3g.

However, on the weekday of the rainy season, more energy is required from the biogas generator as shown in Fig. 3.2a and Fig. 3.2b. The input of RES under this load condition is 44.3% and 44.1%.

3.4. Storage devices input to meet the load demand

In Table 3.11, the energy contributed to satisfying the load demand, from the wind and PV systems, with the support of the storage devices, was considered. To assess the significance of renewable storage in achieving this performance, the contribution of

Table 3.1. Microgrid simulation for Monday during rainy season.

Time Hr	$P_{load}(t)$ MW	$P_{PV}(t)$ MW	$P_w(t)$ MW	$E_h(t)$ MWh	$P_h(t)$ MW	PHS Mode	$E_b(t)$ MWh	$P_b(t)$ MW	Battery Mode	$P_{Bgen}(t)$ MW	$B_{gen.}$ Mode	$P_{ren}(t)$ MW	System(s) Service
12 am	0.60	0.00	0.23	4.00	0.00	0	1.30	0.37	1	0.00	0	0.60	2,4
1 am	0.59	0.00	0.11	3.52	0.48	1	0.93	0.00	0	0.00	0	0.59	2,3
2 am	0.59	0.00	0.05	2.98	0.54	1	0.93	0.00	0	0.00	0	0.59	2,3
3 am	0.60	0.00	0.03	2.41	0.57	1	0.93	0.00	0	0.00	0	0.60	2,3
4 am	0.60	0.00	0.00	1.81	0.60	1	0.93	0.00	0	0.00	0	0.60	3
5 am	0.61	0.00	0.01	1.21	0.60	1	0.93	0.00	0	0.00	0	0.61	3
6 am	0.63	0.00	0.00	0.58	0.63	1	0.93	0.00	0	0.00	0	0.63	3
7 am	0.64	0.05	0.00	0.58	0.00	0	0.93	0.00	0	0.59	1	0.05	1,5
8 am	0.77	0.11	0.04	0.58	0.00	0	0.93	0.00	0	0.62	1	0.15	1,2,5
9 am	0.88	0.16	0.20	0.58	0.00	0	0.93	0.00	0	0.52	1	0.36	1,2,5
10 am	0.99	0.20	0.07	0.58	0.00	0	0.93	0.00	0	0.72	1	0.27	1,2,5
11 am	1.10	0.22	0.10	0.58	0.00	0	0.93	0.00	0	0.78	1	0.32	1,2,5
12 pm	1.11	0.23	0.29	0.58	0.00	0	0.93	0.00	0	0.59	1	0.52	1,2,5
1 pm	1.13	0.22	0.40	0.58	0.00	0	0.93	0.00	0	0.51	1	0.62	1,2,5
2 pm	1.14	0.20	0.34	0.58	0.00	0	0.93	0.00	0	0.60	1	0.54	1,2,5
3 pm	1.14	0.16	0.21	0.58	0.00	0	0.93	0.00	0	0.77	1	0.37	1,2,5
4 pm	1.13	0.11	0.18	0.58	0.00	0	0.93	0.00	0	0.84	1	0.29	1,2,5
5 pm	0.98	0.05	0.12	0.58	0.00	0	0.93	0.00	0	0.81	1	0.17	1,2,5
6 pm	0.85	0.01	0.00	0.58	0.00	0	0.93	0.00	0	0.84	1	0.01	1,5
7 pm	0.72	0.00	0.04	0.58	0.00	0	0.93	0.00	0	0.68	1	0.04	2,5
8 pm	0.63	0.00	0.11	0.58	0.00	0	0.93	0.00	0	0.52	1	0.11	2,5
9 pm	0.64	0.00	0.31	0.58	0.00	0	0.93	0.00	0	0.33	1	0.31	2,5
10 pm	0.62	0.00	0.12	0.58	0.00	0	0.93	0.00	0	0.50	1	0.12	2,5
11 pm	0.59	0.00	0.07	0.58	0.00	0	0.93	0.00	0	0.52	1	0.07	2,5
POWER(MW)	**19.26**	**1.72**	**3.03**							**10.74**		**8.54**	
ENERGY(MWh)	9.63	0.86	1.47							5.37		4.27	

Table 3.2. Microgrid simulation for Wednesday during rainy season.

Time Hr	$P_{load}(t)$ MW	$P_{PV}(t)$ MW	$P_w(t)$ MW	$E_h(t)$ MWh	$P_h(t)$ MW	PHS MW	$E_b(t)$ MWh	$P_b(t)$ MW	Battery Mode	$P_{Bgen}(t)$ MW	$B_{gen.}$ Mode	$P_{ren}(t)$ MW	System(s) Service
12 am	0.68	0.00	0.23	4.00	0.00	0	1.3	0.45	1	0.00	0	0.68	2,4
1 am	0.69	0.00	0.11	3.42	0.58	1	1.3	0.00	0	0.00	0	0.69	2,3
2 am	0.68	0.00	0.05	2.79	0.63	1	1.3	0.00	0	0.00	0	0.68	2,3
3 am	0.66	0.00	0.03	2.16	0.63	1	1.3	0.00	0	0.00	0	0.66	2,3
4 am	0.65	0.00	0.00	1.51	0.65	1	1.3	0.00	0	0.00	0	0.65	3
5 am	0.63	0.00	0.01	0.99	0.62	1	1.3	0.00	0	0.00	0	0.63	2,3
6 am	0.67	0.00	0.00	0.60	0.67	1	1.3	0.00	0	0.00	0	0.67	3
7 am	0.69	0.05	0.00	0.60	0.00	0	1.3	0.00	0	0.64	1	0.05	1,5
8 am	0.77	0.11	0.04	0.60	0.00	0	1.3	0.00	0	0.62	1	0.15	1,2,5
9 am	0.99	0.16	0.20	0.60	0.00	0	1.3	0.00	0	0.63	1	0.36	1,2,5
10 am	1.06	0.20	0.07	0.60	0.00	0	1.3	0.00	0	0.79	1	0.27	1,2,5
11 am	1.1	0.22	0.00	0.60	0.00	0	1.3	0.00	0	0.88	1	0.22	1,5
12 pm	1.11	0.23	0.29	0.60	0.00	0	1.3	0.00	0	0.59	1	0.52	1,2,5
1 pm	1.14	0.22	0.40	0.60	0.00	0	1.3	0.00	0	0.52	1	0.62	1,2,5
2 pm	1.16	0.20	0.34	0.60	0.00	0	1.3	0.00	0	0.62	1	0.54	1,2,5
3 pm	1.17	0.16	0.21	0.60	0.00	0	1.3	0.00	0	0.80	1	0.37	1,2,5
4 pm	1.16	0.11	0.18	0.60	0.00	0	1.3	0.00	0	0.87	1	0.29	1,2,5
5 pm	0.98	0.05	0.12	0.60	0.00	0	1.3	0.00	0	0.81	1	0.17	1,2,5
6 pm	0.87	0.00	0.00	0.60	0.00	0	1.3	0.00	0	0.87	1	0.00	5
7 pm	0.72	0.00	0.04	0.60	0.00	0	1.3	0.00	0	0.68	1	0.04	2,5
8 pm	0.62	0.00	0.11	0.60	0.00	0	1.3	0.00	0	0.51	1	0.11	2,5
9 pm	0.65	0.00	0.31	0.60	0.00	0	1.3	0.00	0	0.34	1	0.31	2,5
10 pm	0.63	0.00	0.12	0.60	0.00	0	1.3	0.00	0	0.51	1	0.12	2,5
11 pm	0.62	0.00	0.07	0.60	0.00	0	1.3	0.00	0	0.55	1	0.07	2,5
POWER(MW)	**20.1**	**1.71**	**2.93**							**11.23**		**8.87**	
ENERGY(MWh)	10.05	0.86	1.47							5.62		4.44	

Table 3.3. Microgrid simulation for Friday during rainy season.

Time Hr	$P_{load}(t)$ MW	$P_{PV}(t)$ MW	$P_w(t)$ MW	$E_h(t)$ MWh	$P_h(t)$ MW	PHS Mode	$E_b(t)$ MWh	$P_b(t)$ MW	Battery Mode	$P_{Bgen}(t)$ MW	$B_{gen.}$ Mode	$P_{ren}(t)$ MW	System(s) Service
12 am	0.59	0.00	0.23	4.00	0.00	0	1.30	0.36	1	0.00	0	0.59	2,4
1 am	0.60	0.00	0.11	3.51	0.49	1	1.30	0.00	0	0.00	0	0.60	2,3
2 am	0.58	0.00	0.05	2.93	0.53	1	1.30	0.00	0	0.00	0	0.58	2,3
3 am	0.56	0.00	0.03	2.37	0.53	1	1.30	0.00	0	0.00	0	0.56	2,3
4 am	0.55	0.00	0.00	1.82	0.55	1	1.30	0.00	0	0.00	0	0.55	3
5 am	0.54	0.00	0.01	1.29	0.53	1	1.30	0.00	0	0.00	0	0.54	2,3
6 am	0.53	0.00	0.00	0.76	0.53	1	1.30	0.00	0	0.00	0	0.53	3
7 am	0.56	0.05	0.00	0.76	0.00	1	1.30	0.00	0	0.51	0	0.05	1,5
8 am	0.67	0.11	0.04	0.76	0.00	1	1.30	0.00	0	0.52	0	0.15	1,2,5
9 am	0.77	0.16	0.20	0.76	0.00	0	1.30	0.00	0	0.41	1	0.36	1,2,5
10 am	0.79	0.20	0.07	0.76	0.00	0	1.30	0.00	0	0.52	1	0.27	1,2,5
11 am	0.80	0.22	0.00	0.76	0.00	0	1.30	0.00	0	0.58	1	0.22	1,5
12 pm	0.64	0.23	0.29	0.76	0.00	0	1.06	0.12	1	0.00	0	0.64	1,2,4
1 pm	0.60	0.22	0.40	0.78	0.00	–1	1.06	0.00	0	0.00	0	0.60	1,2
2 pm	0.58	0.20	0.34	0.74	0.04	0	1.06	0.00	0	0.00	0	0.58	1,2,3
3 pm	0.56	0.16	0.21	0.55	0.19	0	1.06	0.00	0	0.00	0	0.56	1,2,3
4 pm	0.49	0.11	0.18	0.55	0.00	0	1.06	0.00	0	0.20	1	0.29	1,2,5
5 pm	0.42	0.05	0.12	0.55	0.00	0	1.06	0.00	0	0.25	1	0.17	1,2,5
6 pm	0.39	0.00	0.00	0.55	0.00	0	0.67	0.39	1	0.00	0	0.39	4
7 pm	0.38	0.00	0.04	0.55	0.00	0	0.67	0.00	0	0.34	1	0.04	2,5
8 pm	0.36	0.00	0.11	0.55	0.00	0	0.67	0.00	0	0.25	1	0.11	2,5
9 pm	0.36	0.00	0.31	0.55	0.00	0	0.62	0.05	1	0.00	0	0.36	2,4
10 pm	0.37	0.00	0.12	0.55	0.00	0	0.62	0.00	0	0.25	1	0.12	2,5
11 pm	0.37	0.00	0.07	0.55	0.00	0	0.62	0.00	0	0.30	1	0.07	2,5
POWER(MW)	**13.05**	**1.71**	**2.93**							**4.13**		**8.93**	
ENERGY(MWh)	**6.73**	0.86	1.47							2.07		4.47	

Table 3.4. Microgrid simulation for Saturday during rainy season.

Time Hr	$P_{load}(t)$ MW	$P_{PV}(t)$ MW	$P_w(t)$ MW	$E_h(t)$ MWh	$P_h(t)$ MW	PHS Mode	$E_b(t)$ MWh	$P_b(t)$ MW	Battery Mode	$P_{Bgen}(t)$ MW	$B_{gen.}$ Mode	$P_{ren}(t)$ MW	System(s) Service
12 am	0.34	0.00	0.23	4.00	0.00	0	0.96	0.11	1	0.00	0	0.34	2,4
1 am	0.34	0.00	0.11	4.00	0.23	0	0.96	0.00	0	0.00	0	0.34	2,3
2 am	0.35	0.00	0.05	3.77	0.30	1	0.96	0.00	0	0.00	0	0.35	2,3
3 am	0.35	0.00	0.03	3.47	0.32	1	0.96	0.00	0	0.00	0	0.35	2,3
4 am	0.36	0.00	0.00	3.11	0.36	1	0.96	0.00	0	0.00	0	0.36	3
5 am	0.36	0.00	0.01	2.76	0.35	1	0.96	0.00	0	0.00	0	0.36	1,3
6 am	0.38	0.00	0.00	2.38	0.38	1	0.96	0.00	0	0.00	0	0.38	3
7 am	0.42	0.05	0.00	2.01	0.37	1	0.96	0.00	0	0.00	0	0.42	1,3
8 am	0.43	0.11	0.04	1.73	0.28	1	0.96	0.00	0	0.00	0	0.43	1,2,3
9 am	0.46	0.16	0.20	1.63	0.10	1	0.96	0.00	0	0.00	0	0.46	1,2,3
10 am	0.47	0.20	0.07	1.43	0.20	1	0.96	0.00	0	0.00	0	0.47	1,2,3
11 am	0.43	0.22	0.00	1.22	0.21	1	0.96	0.00	0	0.00	0	0.43	1,3
12 pm	0.44	0.23	0.29	1.30	0.00	–1	0.96	0.00	0	0.00	0	0.44	1,2
1 pm	0.45	0.22	0.40	1.47	0.00	–1	0.96	0.00	0	0.00	0	0.45	1,2
2 pm	0.49	0.20	0.34	1.52	0.00	–1	0.96	0.00	0	0.00	0	0.49	1,2
3 pm	0.50	0.16	0.21	1.30	0.00	0	0.83	0.13	1	0.00	0	0.50	1,2,4
4 pm	0.48	0.11	0.18	1.11	0.19	1	0.83	0.00	0	0.00	0	0.48	1,2,3
5 pm	0.47	0.05	0.12	0.81	0.30	1	0.83	0.00	0	0.00	1	0.47	1,2,3
6 pm	0.46	0.00	0.00	0.81	0.00	0	0.83	0.00	0	0.46	1	0.00	5
7 pm	0.45	0.00	0.04	0.81	0.00	0	0.83	0.00	0	0.41	1	0.04	1,5
8 pm	0.42	0.00	0.11	0.81	0.00	0	0.83	0.00	0	0.31	1	0.11	1,5
9 pm	0.41	0.00	0.31	0.81	0.00	0	0.83	0.00	0	0.10	1	0.31	1,5
10 pm	0.40	0.00	0.12	0.81	0.00	0	0.83	0.00	0	0.28	1	0.12	1,5
11 pm	0.39	0.00	0.07	0.81	0.00	0	0.83	0.00	0	0.32	1	0.07	1,5
POWER(MW)	**10.05**	**1.71**	**2.93**							**1.88**		**8.17**	
ENERGY(MWh)	5.03	0.86	1.47							0.94		4.09	

Table 3.5. Microgrid simulation for Sunday during rainy season.

Time Hr	$P_{load}(t)$ MW	$P_{PV}(t)$ MW	$P_w(t)$ MW	$E_h(t)$ MWh	$P_h(t)$ MW	PHS Mode	Eb(t) MWh	$P_b(t)$ MW	Battery Mode	$P_{Bgen}(t)$ MW	$B_{gen.}$ Mode	Pren(t) MW	System(s) Service
12 am	0.36	0.00	0.23	4.00	0.00	0	1.17	0.13	1	0.00	0	0.36	2,4
1 am	0.36	0.00	0.11	4.00	0.00	0	1.17	0.25	1	0.00	0	0.36	2,4
2 am	0.34	0.00	0.05	3.71	0.29	1	1.17	0.00	0	0.00	0	0.34	2,3
3 am	0.32	0.00	0.03	3.42	0.29	1	1.17	0.00	0	0.00	0	0.32	2,3
4 am	0.32	0.00	0.00	3.10	0.32	1	1.17	0.00	0	0.00	0	0.32	3
5 am	0.33	0.00	0.01	3.10	0.32	1	1.17	0.00	0	0.00	0	0.33	2,3
6 am	0.34	0.00	0.00	2.78	0.34	1	1.17	0.00	0	0.00	0	0.34	3
7 am	0.35	0.05	0.00	2.48	0.30	1	1.17	0.00	0	0.00	0	0.35	1,3
8 am	0.36	0.11	0.04	2.27	0.21	1	1.17	0.00	0	0.00	0	0.36	1,2,3
9 am	0.28	0.16	0.20	2.35	0.00	–1	1.17	0.00	0	0.00	0	0.28	1,2
10 am	0.23	0.20	0.07	2.39	0.13	–1	1.17	0.00	0	0.00	0	0.23	1,2
11 am	0.29	0.22	0.00	2.39	0.00	0	1.17	0.07	1	0.00	0	0.29	2,4
12 pm	0.35	0.23	0.29	2.56	0.00	–1	1.17	0.00	0	0.00	0	0.35	1,2
1 pm	0.36	0.22	0.40	2.81	0.00	–1	1.17	0.00	0	0.00	0	0.36	1,2
2 pm	0.38	0.20	0.34	2.97	0.00	–1	1.17	0.00	0	0.00	0	0.38	1,2
3 pm	0.41	0.16	0.21	2.93	0.04	1	1.17	0.00	0	0.00	0	0.41	1,2,3
4 pm	0.44	0.11	0.18	2.78	0.15	1	1.17	0.00	0	0.00	0	0.44	1,2,3
5 pm	0.46	0.05	0.12	2.49	0.29	1	1.17	0.00	0	0.00	0	0.46	1,2,3
6 pm	0.48	0.00	0.00	2.01	0.48	1	1.17	0.00	0	0.00	0	0.48	3
7 pm	0.48	0.00	0.04	1.57	0.44	1	1.17	0.00	0	0.00	0	0.48	2,3
8 pm	0.45	0.00	0.11	1.23	0.34	1	1.17	0.00	0	0.00	0	0.45	2,3
9 pm	0.42	0.00	0.31	1.12	0.11	1	1.17	0.00	0	0.00	0	0.42	2,3
10 pm	0.40	0.00	0.12	0.84	0.28	1	1.17	0.00	0	0.00	0	0.40	2,3
11 pm	0.38	0.00	0.07	0.84	0.00	0	1.17	0.00	0	0.31	1	0.07	1,5
POWER(MW)	**8.89**	**1.71**	**2.93**							**0.31**		**8.58**	
ENERGY(MWh)	4.45	0.86	1.47							0.16		4.29	

Table 3.6. Microgrid simulation for Monday during dry season.

Time Hr	$P_{load}(t)$ MW	$P_{PV}(t)$ MW	$P_w(t)$ MW	$E_h(t)$ MWh	$P_h(t)$ MW	PHS Mode	$E_b(t)$ MWh	$P_b(t)$ MW	Battery Mode	$P_{Bgen}(t)$ MW	$B_{gen.}$ Mode	$P_{ren}(t)$ MW	System(s) Service
12 am	0.60	0.00	0.00	4.00	0.00	0	1.30	0.00	0	0.60	1	0.00	5
1 am	0.59	0.00	0.00	3.61	0.59	1	1.30	0.00	0	0.00	0	0.59	3
2 am	0.59	0.00	0.00	3.21	0.59	1	1.30	0.00	0	0.00	0	0.59	3
3 am	0.60	0.00	0.00	2.81	0.60	1	1.30	0.00	0	0.00	0	0.60	3
4 am	0.60	0.00	0.00	2.41	0.60	1	1.30	0.00	0	0.00	0	0.60	3
5 am	0.61	0.01	0.00	2.01	0.60	1	1.30	0.00	0	0.00	0	0.61	3
6 am	0.63	0.07	0.00	1.59	0.56	1	1.30	0.00	0	0.00	0	0.63	1,3
7 am	0.64	0.16	0.00	1.18	0.48	1	1.30	0.00	0	0.00	0	0.64	1,3
8 am	0.77	0.27	0.03	1.18	0.40	0	1.30	0.00	0	0.00	0	0.77	1,2,3
9 am	0.88	0.31	0.08	0.78	0.00	0	0.80	0.50	0	0.00	0	0.88	1,2,4
10 am	0.99	0.37	0.04	0.78	0.00	0	0.80	0.00	0	0.58	1	0.41	1,2,5
11 am	1.10	0.40	0.06	0.78	0.00	0	0.80	0.00	0	0.63	1	0.46	1,2,5
12 pm	1.11	0.42	0.02	0.78	0.00	0	0.80	0.00	0	0.67	1	0.44	1,2,5
1 pm	1.13	0.49	0.01	0.78	0.00	0	0.80	0.00	0	0.63	1	0.50	1,2,5
2 pm	1.14	0.52	0.02	0.78	0.00	0	0.80	0.00	0	0.60	1	0.54	1,2,5
3 pm	1.14	0.52	0.00	0.78	0.00	0	0.80	0.00	0	0.62	1	0.52	1,5
4 pm	1.13	0.49	0.00	0.78	0.00	0	0.80	0.00	0	0.64	1	0.49	1,5
5 pm	0.98	0.40	0.00	0.78	0.00	0	0.80	0.00	0	0.57	1	0.40	1,5
6 pm	0.85	0.35	0.00	0.78	0.00	0	0.80	0.00	0	0.50	1	0.35	1,5
7 pm	0.72	0.12	0.00	0.78	0.00	0	0.80	0.00	0	0.60	1	0.12	1,5
8 pm	0.63	0.06	0.00	0.78	0.00	0	0.80	0.00	0	0.57	1	0.06	1,5
9 pm	0.64	0.00	0.00	0.78	0.00	0	0.80	0.00	0	0.64	1	0.00	5
10 pm	0.62	0.00	0.00	0.78	0.00	0	0.80	0.00	0	0.62	1	0.00	5
11 pm	0.59	0.00	0.00	0.78	0.00	0	0.80	0.00	0	0.59	1	0.00	5
POWER(MW)	**19.26**	**4.96**	**0.26**							**9.06**		**10.20**	
ENERGY(MWh)	9.63	2.48	0.13							4.53		5.10	

Table 3.7. Microgrid simulation for Wednesday during dry season.

Time Hr	$P_{load}(t)$ MW	$P_{PV}(t)$ MW	$P_w(t)$ MW	$E_h(t)$ MWh	$P_h(t)$ MW	PHS MW	$E_b(t)$ MWh	$P_b(t)$ MW	Battery Mode	$P_{Bgen}(t)$ MW	$B_{gen.}$ Mode	$P_{ren}(t)$ MW	System(s) Service
12 am	0.68	0.00	0.00	4.00	0.00	0	0.62	0.68	0	0.00	0	0.68	4
1 am	0.69	0.00	0.00	3.31	0.69	1	0.62	0	0	0.00	0	0.69	3
2 am	0.68	0.00	0.00	2.63	0.68	1	0.62	0	0	0.00	0	0.68	3
3 am	0.66	0.00	0.00	1.97	0.66	1	0.62	0	0	0.00	0	0.66	3
4 am	0.65	0.00	0.00	2.21	0.65	1	0.62	0	0	0.00	0	0.65	3
5 am	0.63	0.01	0.00	1.79	0.62	1	0.62	0	0	0.00	0	0.63	1,3
6 am	0.67	0.07	0.00	1.35	0.60	1	0.62	0	0	0.00	0	0.67	1,3
7 am	0.69	0.16	0.00	0.95	0.53	0	0.62	0	0	0.00	0	0.69	1,3
8 am	0.77	0.27	0.03	0.95	0.00	0	0.62	0	0	0.47	1	0.30	1,2,5
9 am	0.99	0.31	0.08	0.95	0.00	0	0.62	0	0	0.60	1	0.39	1,2,5
10 am	1.06	0.37	0.04	0.95	0.00	0	0.62	0	0	0.65	1	0.41	1,2,5
11 am	1.10	0.40	0.06	0.95	0.00	0	0.62	0	0	0.64	1	0.46	1,2,5
12 pm	1.11	0.42	0.02	0.95	0.00	0	0.62	0	0	0.67	1	0.44	1,2,5
1 pm	1.14	0.49	0.01	0.95	0.00	0	0.62	0	0	0.64	1	0.50	1,2,5
2 pm	1.16	0.52	0.02	0.95	0.00	0	0.62	0	0	0.62	1	0.54	1,2,5
3 pm	1.17	0.52	0.00	0.95	0.00	0	0.62	0	0	0.65	1	0.52	1,5
4 pm	1.16	0.49	0.00	0.95	0.00	0	0.62	0	0	0.67	1	0.49	1,5
5 pm	0.98	0.40	0.00	0.95	0.00	0	0.62	0	0	0.58	1	0.40	1,5
6 pm	0.87	0.35	0.00	0.95	0.00	0	0.62	0	0	0.52	1	0.35	1,5
7 pm	0.72	0.12	0.00	0.95	0.00	0	0.62	0	0	0.60	1	0.12	1,5
8 pm	0.62	0.06	0.00	0.95	0.00	0	0.62	0	0	0.56	1	0.06	5
9 pm	0.65	0.00	0.00	0.95	0.00	0	0.62	0	0	0.65	1	0.00	5
10 pm	0.63	0.00	0.00	0.95	0.00	0	0.62	0	0	0.63	1	0.00	5
11 pm	0.62	0.00	0.00	0.95	0.00	0	0.62	0	0	0.62	1	0.00	5
POWER(MW)	**20.10**	**4.96**	**0.26**							**9.77**		**10.33**	
ENERGY(MWh)	10.05	2.48	0.13							6.07		3.99	

Table 3.8. Microgrid simulation for Friday during dry season.

Time Hr	$P_{load}(t)$ MW	$P_{PV}(t)$ MW	$P_w(t)$ MW	$E_h(t)$ MWh	$P_h(t)$ MW	PHS Mode	Eb(t) MWh	$P_b(t)$ MW	Battery Mode	$P_{Bgen}(t)$ MW	$B_{gen.}$ Mode	Pren(t) MW	System(s) Service
12 am	0.59	0.00	0.00	4.00	0.00	0	1.30	0.00	0	0.59	1	0.00	5
1 am	0.60	0.00	0.00	3.40	0.60	1	1.30	0.00	0	0.00	0	0.60	3
2 am	0.58	0.00	0.00	2.82	0.58	1	1.30	0.00	0	0.00	0	0.58	3
3 am	0.56	0.00	0.00	2.26	0.56	1	1.30	0.00	0	0.00	0	0.56	3
4 am	0.55	0.00	0.00	1.70	0.56	1	1.30	0.00	0	0.00	0	0.55	3
5 am	0.54	0.01	0.00	1.70	0.00	0	0.77	0.53	1	0.00	0	0.54	1,4
6 am	0.53	0.07	0.00	1.24	0.46	1	0.77	0.00	0	0.00	0	0.53	1,3
7 am	0.56	0.16	0.00	0.84	0.40	1	0.77	0.00	0	0.00	0	0.56	1,3
8 am	0.67	0.27	0.03	0.47	0.37	1	0.77	0.00	0	0.00	0	0.67	1,3
9 am	0.77	0.31	0.08	0.47	0.00	0	0.77	0.00	0	0.38	1	0.39	1,2,5
10 am	0.79	0.37	0.04	0.47	0.00	0	0.77	0.00	0	0.38	1	0.42	1,2,5
11 am	0.80	0.40	0.06	0.47	0.00	0	0.77	0.00	0	0.34	1	0.46	1,2,5
12 pm	0.64	0.42	0.02	0.47	0.00	0	0.77	0.00	0	0.20	1	0.44	1,2,5
1 pm	0.60	0.49	0.01	0.47	0.00	0	0.77	0.00	0	0.10	1	0.50	1,2,5
2 pm	0.58	0.52	0.02	0.47	0.00	0	0.77	0.00	0	0.04	1	0.54	1,2,5
3 pm	0.56	0.52	0.00	0.43	0.04	1	0.77	0.00	0	0.00	0	0.56	1,2,3
4 pm	0.49	0.49	0.00	0.43	0.00	0	0.77	0.00	0	0.00	0	0.49	1
5 pm	0.42	0.40	0.00	0.41	0.02	1	0.77	0.00	0	0.00	0	0.40	1,3
6 pm	0.39	0.35	0.00	0.41	0.00	0	0.77	0.00	0	0.04	1	0.35	1,5
7 pm	0.38	0.12	0.00	0.41	0.00	0	0.77	0.00	0	0.26	1	0.12	1,5
8 pm	0.36	0.06	0.00	0.41	0.00	0	0.77	0.00	0	0.30	1	0.06	1,5
9 pm	0.36	0.00	0.00	0.41	0.00	0	0.77	0.00	0	0.36	1	0.00	5
10 pm	0.37	0.00	0.00	0.41	0.00	0	0.77	0.00	0	0.37	1	0.00	5
11 pm	0.37	0.00	0.00	0.41	0.00	0	0.77	0.00	0	0.37	1	0.00	5
POWER(MW)	**13.05**	**4.96**	**0.26**							**3.73**		**9.32**	
ENERGY(MWh)	6.53	2.48	0.13							1.87		4.66	

Table 3.9. Microgrid simulation for Saturday during dry season.

Time Hr	$P_{load}(t)$ MW	$P_{PV}(t)$ MW	$P_w(t)$ MW	$E_h(t)$ MWh	$P_h(t)$ MW	PHS MW	Eb(t) MWh	$P_b(t)$ MW	Battery Mode	$P_{Bgen}(t)$ MW	$B_{gen.}$ Mode	Pren(t) MW	System(s) Service
12 am	0.34	0.00	0.00	4.00	0.00	0	0.96	0.34	1	0.00	0	0.34	4
1 am	0.34	0.00	0.00	4.00	0.00	0	0.96	0.00	0	0.34	1	0.00	5
2 am	0.35	0.00	0.00	3.65	0.35	1	0.96	0.00	0	0.00	0	0.35	3
3 am	0.35	0.00	0.00	3.18	0.35	1	0.96	0.00	0	0.00	0	0.35	3
4 am	0.36	0.00	0.00	2.93	0.36	1	0.96	0.00	0	0.00	0	0.36	3
5 am	0.36	0.01	0.00	2.58	0.35	1	0.96	0.00	0	0.00	0	0.36	1,3
6 am	0.38	0.07	0.00	2.27	0.31	1	0.96	0.00	0	0.00	0	0.38	1,3
7 am	0.42	0.16	0.00	2.01	0.26	1	0.96	0.00	0	0.00	0	0.42	1,3
8 am	0.43	0.27	0.03	1.78	0.23	1	0.96	0.00	0	0.00	0	0.43	1,2,3
9 am	0.46	0.31	0.08	1.78	0.00	1	0.89	0.07	1	0.00	0	0.46	1,2,4
10 am	0.47	0.37	0.04	1.72	0.06	1	0.89	0.00	0	0.00	0	0.47	1,2,3
11 am	0.43	0.40	0.06	1.72	0.00	1	0.89	0.00	0	0.00	0	0.43	1,2
12 pm	0.44	0.42	0.02	1.63	0.09	1	0.89	0.00	0	0.00	0	0.44	1,2
1 pm	0.45	0.49	0.01	1.64	0.00	–1	0.93	0.04	–1	0.00	0	0.45	1
2 pm	0.49	0.52	0.02	1.66	0.18	–1	0.96	0.03	–1	0.00	0	0.49	1
3 pm	0.50	0.52	0.00	1.66	0.00	0	0.98	0.02	–1	0.00	0	0.50	1
4 pm	0.48	0.49	0.00	1.66	0.00	0	0.99	0.01	–1	0.00	0	0.48	1
5 pm	0.47	0.40	0.00	1.59	0.07	1	0.99	0.00	0	0.00	0	0.47	1,3
6 pm	0.46	0.35	0.00	1.48	0.11	1	0.99	0.00	0	0.00	0	0.46	1,3
7 pm	0.45	0.12	0.00	1.15	0.33	1	0.99	0.00	0	0.00	0	0.45	1,3
8 pm	0.42	0.06	0.00	1.15	0.00	0	0.99	0.00	0	0.36	1	0.06	1,5
9 pm	0.41	0.00	0.00	1.15	0.00	0	0.99	0.00	0	0.41	1	0.00	5
10 pm	0.40	0.00	0.00	1.15	0.00	0	0.99	0.00	0	0.40	1	0.00	5
11 pm	0.39	0.00	0.00	1.15	0.00	0	0.99	0.00	0	0.39	1	0.00	5
POWER(MW)	**10.05**	**4.96**	**0.26**							**1.90**		**8.15**	
ENERGY(MWh)	5.03	2.48	0.13							0.95		4.08	

Table 3.10. Microgrid simulation for Sunday during dry season.

Time Hr	$P_{load}(t)$ MW	$P_{PV}(t)$ MW	$P_w(t)$ MW	$E_h(t)$ MWh	$P_h(t)$ MW	PHS MW	$E_b(t)$ MWh	$P_b(t)$ MW	Battery Mode	$P_{Bgen}(t)$ MW	$B_{gen.}$ Mode	$P_{ren}(t)$ MW	System(s) Service
12 am	0.36	0.00	0.00	4.00	0.00	0	0.94	0.36	1	0.00	0	0.36	4
1 am	0.36	0.00	0.00	3.64	0.36	1	0.94	0.00	0	0.00	0	0.36	3
2 am	0.34	0.00	0.00	3.30	0.34	1	0.94	0.00	0	0.00	0	0.34	3
3 am	0.32	0.00	0.00	2.98	0.32	1	0.94	0.00	0	0.00	0	0.32	3
4 am	0.32	0.00	0.00	2.66	0.32	1	0.94	0.00	0	0.00	0	0.32	3
5 am	0.33	0.01	0.00	2.33	0.33	1	0.94	0.00	0	0.00	0	0.33	3
6 am	0.34	0.07	0.00	2.06	0.27	1	0.94	0.00	0	0.00	0	0.34	1,3
7 am	0.35	0.16	0.00	1.87	0.19	1	0.94	0.00	0	0.00	0	0.35	1,3
8 am	0.36	0.27	0.03	1.81	0.06	1	0.94	0.00	0	0.00	0	0.36	1,2,3
9 am	0.28	0.31	0.08	1.89	0.00	–1	0.97	0.04	–1	0.00	0	0.28	1
10 am	0.23	0.37	0.04	1.93	0.00	–1	1.02	0.14	–1	0.00	0	0.23	1
11 am	0.29	0.40	0.06	1.87	0.00	–1	1.13	0.11	–1	0.00	0	0.29	1
12 pm	0.35	0.42	0.02	1.89	0.00	–1	1.2	0.07	–1	0.00	0	0.35	1
1 pm	0.36	0.49	0.01	2.00	0.00	–1	1.33	0.13	–1	0.00	0	0.36	1
2 pm	0.38	0.52	0.02	2.02	0.00	–1	1.47	0.14	–1	0.00	0	0.38	1
3 pm	0.41	0.52	0.00	2.02	0.00	0	1.58	0.11	–1	0.00	0	0.41	1
4 pm	0.44	0.49	0.00	2.02	0.00	0	1.63	0.05	–1	0.00	0	0.44	1
5 pm	0.46	0.40	0.00	2.02	0.00	1	1.57	0.06	1	0.00	0	0.46	1,4
6 pm	0.48	0.35	0.00	1.89	0.13	1	1.57	0.00	0	0.00	0	0.48	1,3
7 pm	0.48	0.12	0.00	1.53	0.36	1	1.57	0.00	0	0.00	0	0.48	1,3
8 pm	0.45	0.06	0.00	1.14	0.39	1	1.57	0.00	0	0.00	0	0.45	1,3
9 pm	0.42	0.00	0.00	0.72	0.42	1	1.57	0.00	0	0.00	1	0.42	3
10 pm	0.4	0.00	0.00	0.72	0.00	0	1.57	0.00	0	0.40	1	0.00	3
11 pm	0.38	0.00	0.00	0.72	0.00	0	1.57	0.00	0	0.38	1	0.00	5
POWER(MW)	**8.89**	**4.96**	**0.26**							**0.78**		**8.11**	
ENERGY(MWh)	4.45	2.48	0.13							0.39		4.06	

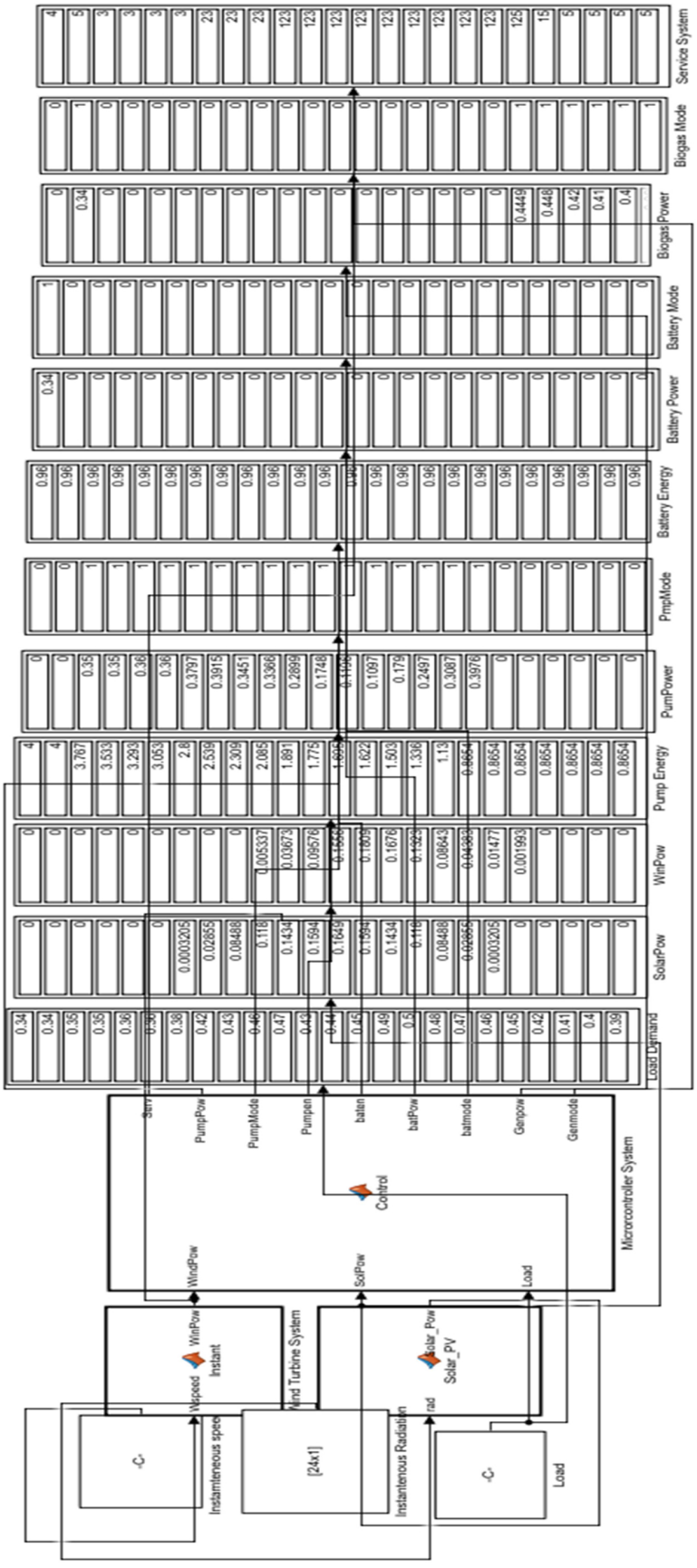

Fig. 3.1. Screenshot of Microcontroller system.

Table 3.11. Contributions of energy sources under different scenarios.

Scenario	E_{load} (MWh)	E_{ren} (MWh)	E_{ren} %	E_{Bgen} (MWh)	E_{Bgen} %
June - MON – AS	9.63	4.27	44.3	5.37	55.8
June - WED – AS	10.05	4.44	44.1	5.62	55.9
June - FRI – AS	6.73	4.47	66.4	2.07	30.8
June - SAT – AS	5.03	4.09	81.3	0.94	18.7
June - SUN – AS	4.45	4.29	96.4	0.16	3.59
December -MON– AS	9.63	5.10	53.0	4.53	47.0
December -WED– AS	10.05	5.17	51.4	4.89	48.7
December -FRI– AS	6.53	4.66	71.4	1.87	28.6
December-SAT– AS	5.03	4.08	81.1	0.95	18.9
December-SUN– AS	4.45	4.06	91.2	0.39	8.76

the storage subsystem was evaluated through its charging and discharging profiles, cumulative energy throughput, and its influence on key reliability indices. Specifically, the simulations tracked how much surplus wind and solar energy was absorbed by the battery and pumped-hydro units, how much of this stored energy was later used to supply the load, and how these interactions affected curtailed renewable energy, backup biogas usage, and the loss of power supply probability. This analysis provides a direct measure of how the storage subsystem enables optimum utilization of wind and solar resources while maintaining an LPSP of zero. The storage devices' net energy contribution to meeting the site's load demand is estimated from Eq. (3.1):

$$E_{sto} = \left(E_{ph} + E_b\right) = E_{load} - \left(E'_{ren} + E_{Bgen}\right) \tag{3.1}$$

Where E'_{ren} is the net energy generation from the two energy sources (wind and PV systems) as indicated in Eq. (3.2):

$$E'_{ren} = \sum_{n=1}^{24} (P_w + P_{PV})T \tag{3.2}$$

Eq. (3.3) calculates the percentage energy input of the storage system to satisfy the load:

$$E_{ren}\,(\%) = \frac{E_{ren}}{E_{load}} 100\% \tag{3.3}$$

Table 3.12 shows the percentage input of storage devices to satisfy the load demand in various scenarios. At various conditions, the storage devices contributed 20.0 % to 44.0% of the total energy demand of the site under investigation, with values ranging from 1.45 MWh to 2.56 MWh. These are enormous energy values that the battery itself cannot manage, both technically and economically [30]. As a result, pumped hydro storage enables optimal utilization of renewable energy, particularly in an HRES with high wind energy penetration. With PHSS, there exists a significant storage capacity for surplus energy, which can be utilized later when the need arises.

Figs. 3.4 and 3.5 show that in most of the cases studied, pumped hydro stands out as the most dynamic storage facility. The changes in the battery's energy content, at both charging and discharging modes, are small and they happen within short time intervals. The battery is in standby mode most of the time. The changes in the pumped-hydro storage are significant and happen over a wide interval of time. According to the simulation results, the ESS is mostly in generation mode. Fig. 3.4 (d and e) show, however, that the rainy season (June) has the potential to produce surplus RE, which can be stored. This is because of the high wind speed this month. When this excess energy when stored over a considerable period, it becomes sufficient for usage at other periods that have less RE potential, such as the dry season (Fig. 3.4).

As illustrated in Figs. 3.4 and 3.5, pumped hydro storage offers an effective solution for storing surplus energy to be utilized at a later time, whereas the battery action is restricted to providing short-term support for pumped-hydro storage, particularly prior to the period the pumped-hydro can begin to generate.

As illustrated in Figs. 3.4 and 3.5, pumped hydro storage offers an effective solution for storing surplus energy to be utilized at a later time, whereas the battery action is restricted to providing short-term support for pumped-hydro storage, particularly prior to the period the pumped-hydro can begin to generate. The pumped-hydro storage has a high energy density, however, the response time is slow, whereas the battery has a low energy density but a faster response time than the pumped-hydro storage.

3.5. Economic analysis of the system

In this study, a feasibility study was conducted, and a comparative analysis of various system models

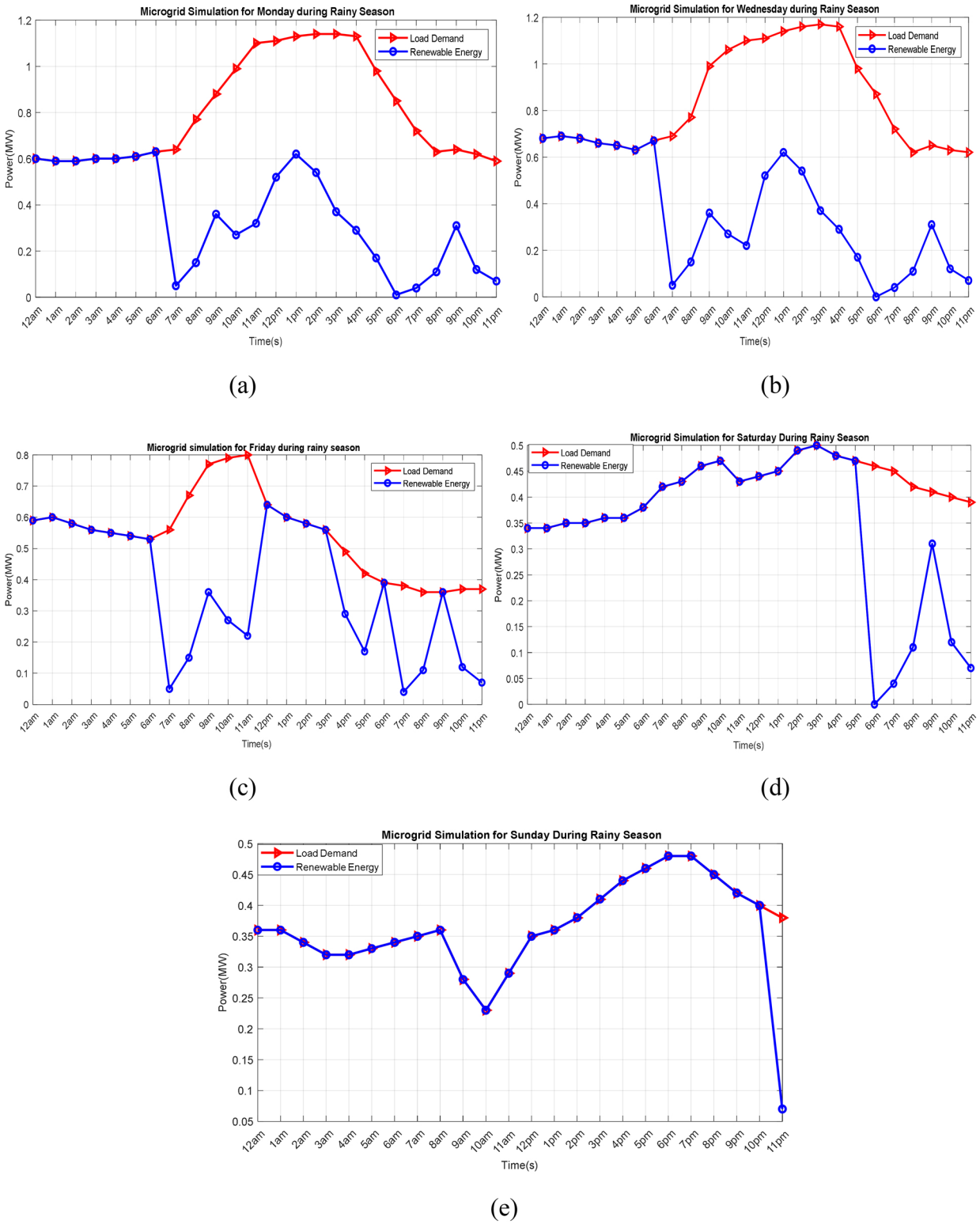

Fig. 3.2. Power Contribution from the Renewable Sources towards Meeting Load Demand in June (a) Monday (b) Wednesday (c) Friday (d) Saturday (e) Sunday.

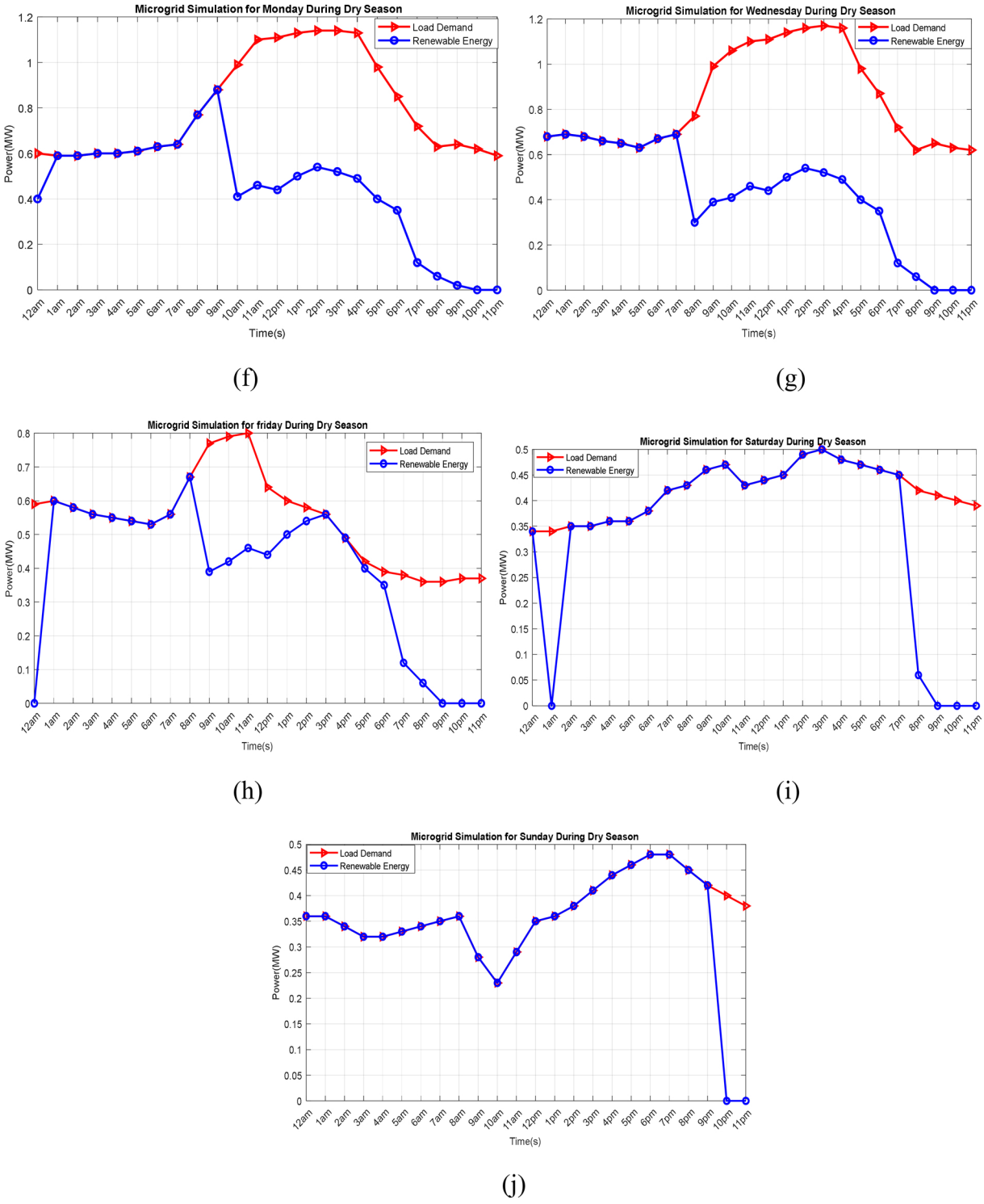

Fig. 3.3. Power Contribution from the Renewable Sources Towards Meeting Load Demand in December (f) Monday (g) Wednesday (h) Friday (i) Saturday (j) Sunday.

was carried out to identify the optimal system while also validating the proposed standalone scheme. The comparative analysis involved simulating various system configurations previously studied in the literature under different loads, input settings, and locations. However, in this study, only the design configuration ideas of these systems were considered.

Table 3.12. Contributions of storage facilities under different scenarios.

Scenario	E_{load} (MWh)	E_{Bgen} (MWh)	E'_{ren} (MWh)	E_{sto} (MWh)	E_{sto} (%)
June - MON – AS	9.63	5.37	2.33	1.94	20.1
June - WED – AS	10.05	5.62	2.33	2.11	21.0
June - FRI – AS	6.73	2.07	2.33	2.14	31.8
June - SAT – AS	5.03	0.94	2.33	1.76	35.0
June - SUN – AS	4.45	0.16	2.33	1.96	44.0
December - MON – AS	9.63	4.53	2.61	2.49	25.9
December - WED – AS	10.05	4.89	2.61	2.56	25.5
December - FRI – AS	6.53	1.87	2.61	2.05	31.4
December - SAT – AS	5.03	0.95	2.61	1.47	29.2
December - SUN – AS	4.45	0.39	2.61	1.45	32.6

3.5.1. Fixed costs

The fixed (installation) costs of the HRES are calculated below:

The annualized (O & M) cost is obtained by taking 10% of the annualized capital cost (due to the biogas generator and other auxiliary components):

$$C_{o\&m} = 124{,}030 \times 0.1 = \$12{,}403/\text{year} \tag{3.4}$$

The HRES average year of use is calculated to be 26.5 years.

$$Year_{ave} = \frac{\sum_{n=1}^{5} Y}{5} \tag{3.5}$$

Hence, the total (O & M) cost over 26.5 years is:

$$C_{o\&m} = 12{,}403 \times 26.5 = \$328{,}679.5/\text{year} \tag{3.6}$$

The total cost of installation of the HRES for a projected average lifetime of 26.5 years is:

$$C_{inst} = C_k + C_{o\&m} \tag{3.7}$$

$$C_{inst} = 2{,}938{,}750 + 328{,}679.5 = \$3{,}267{,}429.5$$

3.6. Systems optimization and selection scenarios

The current study utilizes SQP to attain diverse HRES topologies in three different ways: simulation, optimization, and sensitivity analysis. The economic parameters obtained from the optimization method, including the minimum NPC and LCOE, were used to rank and select the best off-grid HRES design. Furthermore, a techno-economic analysis of a standalone HRES system, including sensitivity parameters, is performed to determine the best system for the location under consideration. The simulation results are determined by the input parameters of the component, peak load demand, cost, and other constraints, as shown in Table 2.1 above. Furthermore, it generates a large number of HRES systems that are suitable and effective for satisfying the load requirements at the target location.

Tables 3.13 and 3.14 display the configuration of the hybrid system derived from the analysis conducted through simulation. The system configurations include PV/wind turbine/pumped hydro/battery/biogas, PV/wind/battery, and Wind/pumped hydro/biogas. Table 3.13 shows that the PV/Wind/Pumped Hydro/Battery/Biogas configuration is more cost-effective than other configurations. The optimal system consists of a 400-kW wind turbine and a 500-kW PV system.

Cost analysis of the optimal HRES

The economic analysis uses a 25-year project lifetime and a real discount rate of 8% to compute component-level Net Present Cost (NPC). For the solar PV and wind subsystems, we assume lifetimes of 25 years with annual O&M of 1.0% and 2.0% of capital respectively. The battery–inverter system is assumed to require a full replacement at year 10 (replacement cost $180,000) with an annual O&M of $3,145, and an end-of-project salvage value of $95,094. Biogas plant economics include both a replacement/overhaul at year 12 ($190,342.70) and recurring fuel costs (annualized to $28,589.5 PV). Pumped hydro is modelled as long-lived infrastructure (no major replacement within 25 years) with periodic minor refurbishment ($7,600). All cash flows are discounted to present value and summed up to obtain the NPC for each component and for the system

The techno-economic evaluation of the proposed HRES shows a total net present cost (NPC) of 3,085,675.2$, which reflects the combined effect of capital, O&M, fuel, replacement, and salvage terms over the project lifetime. Capital cost dominates the NPC, with a total of 2,792,000$. Solar PV (1,250,000$) and biogas (611,000$) are the main contributors, while wind, pumped hydro, and the battery–inverter subsystem play supporting roles in reliability and storage. Annual O&M expenses are

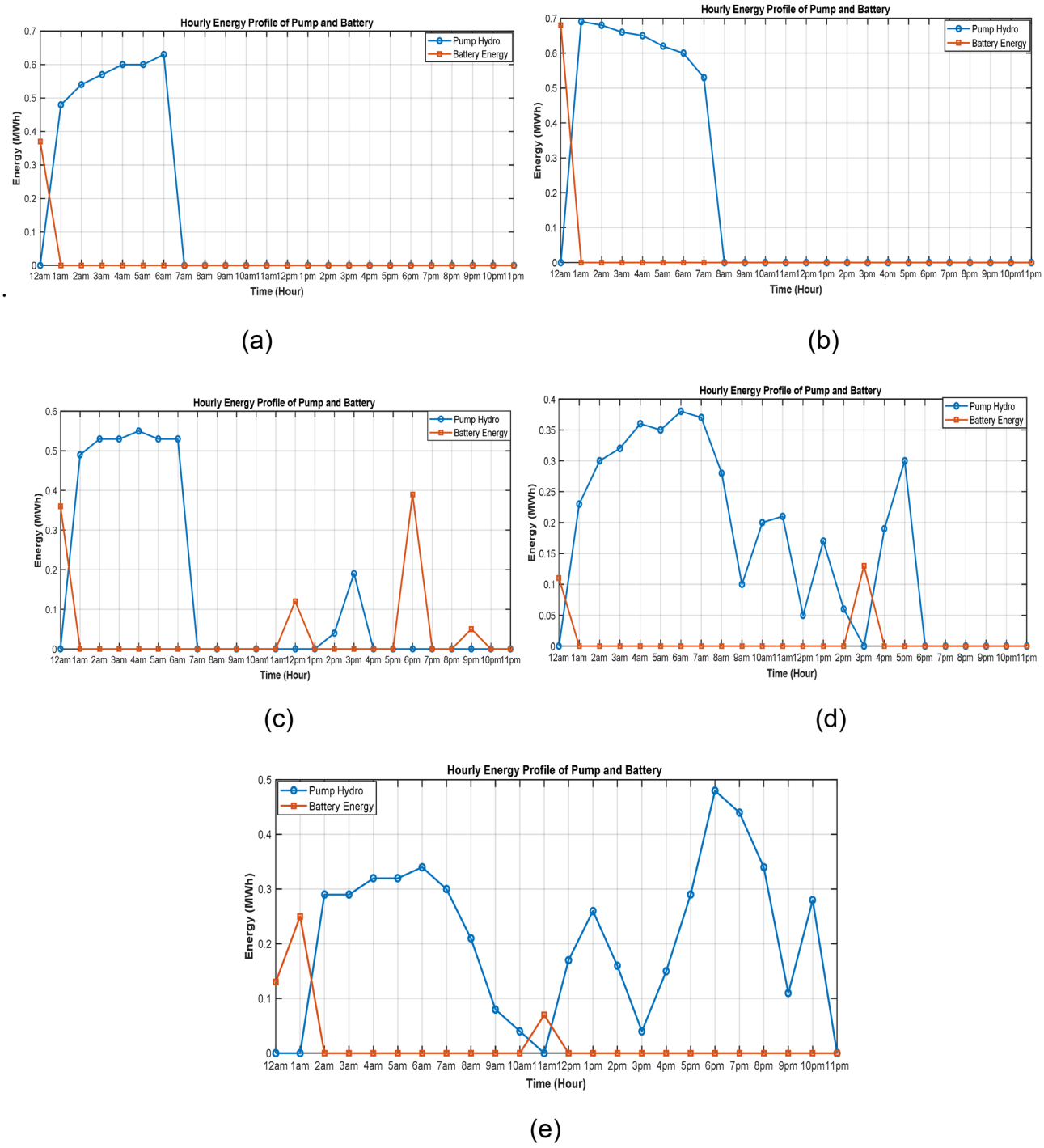

Fig. 3.4. Energy Cycle for the Storage in June (a) Monday (b) Wednesday (c) Friday (d) Saturday (e) Sunday.

relatively small (44,065$ in total), indicating that the lifecycle cost is largely driven by the initial investment rather than recurrent operation. Replacement costs reach 377,942.7$, mainly due to the inverter and biogas units, highlighting the importance of component lifetime in overall economics. Fuel cost is modest (28,589.5$) and is almost entirely associated with the biogas subsystem, whereas solar and wind operate without fuel expenditure. A salvage value of 148,522$ partially offsets the lifecycle cost, with the largest contributions coming from the battery–inverter and biogas components.

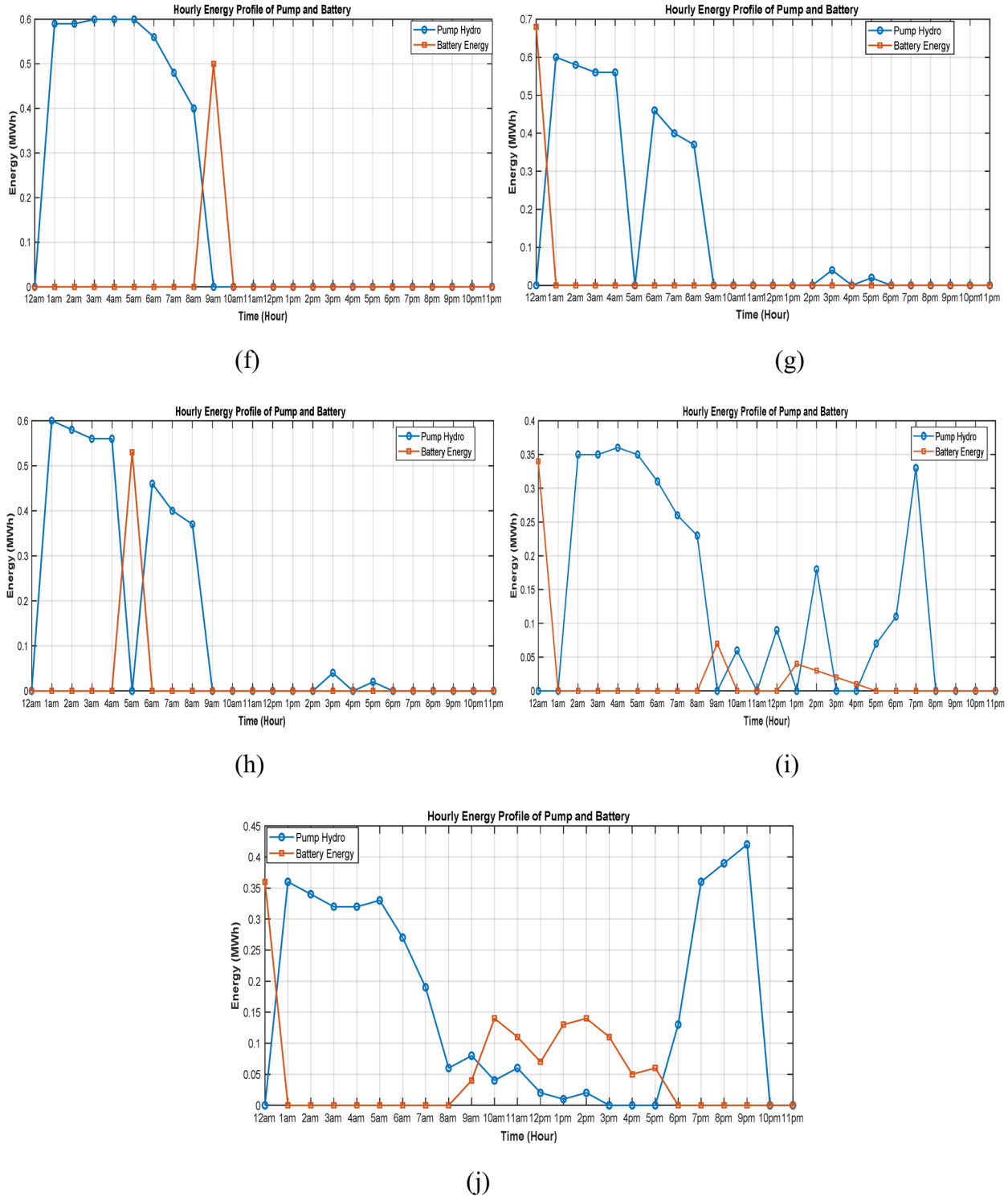

Fig. 3.5. Energy Cycle for the Storage in December (f) Monday (g) Wednesday (h) Friday (e) Saturday (f) Sunday.

Overall, solar PV and biogas together account for about two-thirds of the NPC, confirming their role as the dominant cost drivers and primary energy providers in the HRES. The strong influence of capital and replacement costs suggests that future cost-reduction efforts should focus on optimal sizing of these units and on selecting technologies with longer lifetimes and lower replacement requirements.

Table 3.13. Cost breakdown of the best HRES.

Component	Net capital Cost *Ck* ($)	O & M Cost ($)	Replacement Cost ($)	Fuel cost ($)	Salvage Cost ($)	Net Present Cost ($)
Wind Turbine	600,000	12,000	0.0	0.0	0.0	**612,000.0**
Solar PV	1,250,000	12,500	0.0	0.0	0.0	**1,262,500.0**
Pumped Hydro	140,000	4,200	7,600.0	0.0	6,739.6	**136,660.4**
Battery with Inverter	191,000	3,145	180,000.0	0.0	95,094.3	**279,050.7**
Biogas	611,000	12,220	190,342.7	28,589.5	46,688.1	**795,464.1**
Total	**2,792,000**	**44,065**	**377,942.7**	**28,589.5**	**148,522.00**	**3,085,675.2**

Table 3.14. Configuration B.

Component	Net capital Cost *Ck* ($)	O & M Cost ($)	Replacement Cost ($)	Fuel cost ($)	Salvage Cost ($)	Net Present Cost ($/yr.)
Wind Turbine	600,000	12,000	0.0	0.0	0.0	**612,000**
Solar PV	2,250,000	33,750	0.0	0.0	0.0	**2,283,750**
Battery with Inverter	250,000	15,750	205,882.4	0.0	108,768.1	**362,864**
Total	**3,100,000**	**61,500**	**205,882**	0.0	**108,768.10**	**3,258,614**

Table 3.14. Configuration C.

Component	Net capital Cost *Ck*	O & M Cost	Replacement Cost $	Fuel cost $	Salvage Cost $	Net Present Cost ($/yr.)
Wind Turbine	1,425,000	42,750	0.0	0.0	0.0	**1,467,750.0**
Pumped Hydro	210,000	13,500	288,235.3	0.0	4,580.6	**635,860.4**
Biogas	705,000	42,300	270,246.0	60,159.0	24,320.8	**1,117,284.0**
Total	**2,340,000**	**98,550**	**558,481**	**60,159**	**28,901.40**	**3,220,894.4**

3.7. Comparison of configuration for economic power systems

Table 3.13 displays the cost-effective system as a categorized simulation result. Configurations were compared while keeping the constraint values constant across all system configurations. The best energy system was chosen based on its NPC, LCOE, and lower fuel consumption.

3.7.1. Based on total net present cost

Table 3.13 shows that the configuration of HRES of configuration A, which comprises wind, solar PV, pumped hydro, battery, and biogas as shown in Fig. 3.6, has the lowest net present cost of $3,085,675 while the configurations (B & C) are $3,258,614 and $3,220,895, respectively. The detail of NPC is shown in Fig. 3.6.

3.7.2. Based on levelized cost of energy

Refer to Fig. 3.7 and Table 3.15 for detailed information on the LCOE for each power system configuration. Three configurations, A, B, and C, have nearly identical energy costs with minor differences, but configuration A has the lowest value of all configurations. The LCOE for configuration A is around $0.027/kWh, $0.029/kWh for configuration B, and $0.028/kWh for configuration C. Using this parameter as a benchmark comparison, configuration A provides the best optimal economic costs for the optimization algorithm in terms of LCOE.

3.7.3. Based on fuel consumption

For this study, the biogas fuel cost used in the calculation was based on [31]. From the listed situations, configuration A has the lowest biogas fuel consumption which is about $28,589.5; configuration B has no biogas in the configuration, whereas configuration C has consumed about $60,159 which is higher than configuration A due to the increasing usage of biogas to meet the load demand which resulted from the period of unavailability of RES. Variations in fuel consumption by the two configurations are depicted in Fig. 3.8. Biogas was used because it emits the lowest greenhouse gases when compared to other fuels. It can be used in rural distributed generation systems where natural gas availability may be limited. Compared to natural gas, biogas plays a crucial role in waste decontamination by capturing methane emitted from organic waste decomposition, a potent greenhouse gas that would otherwise contribute to air pollution. This process not only limits harmful emissions but also reduces soil and water contamination by preventing landfill leachate and producing nutrient-rich digestate that can be used as fertilizer. Additionally, biogas has a significantly lower

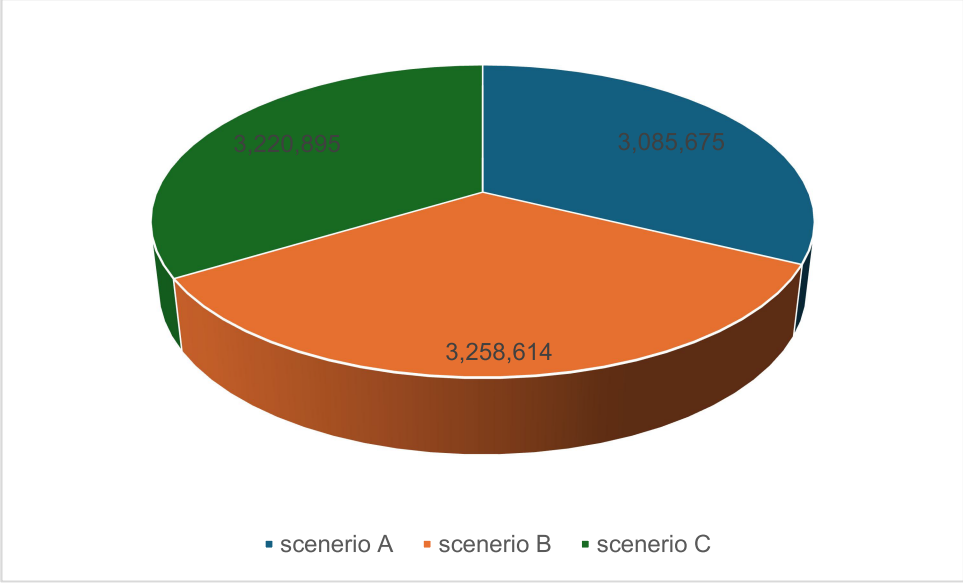

Fig. 3.6. Comparison of Configuration Based on NPC.

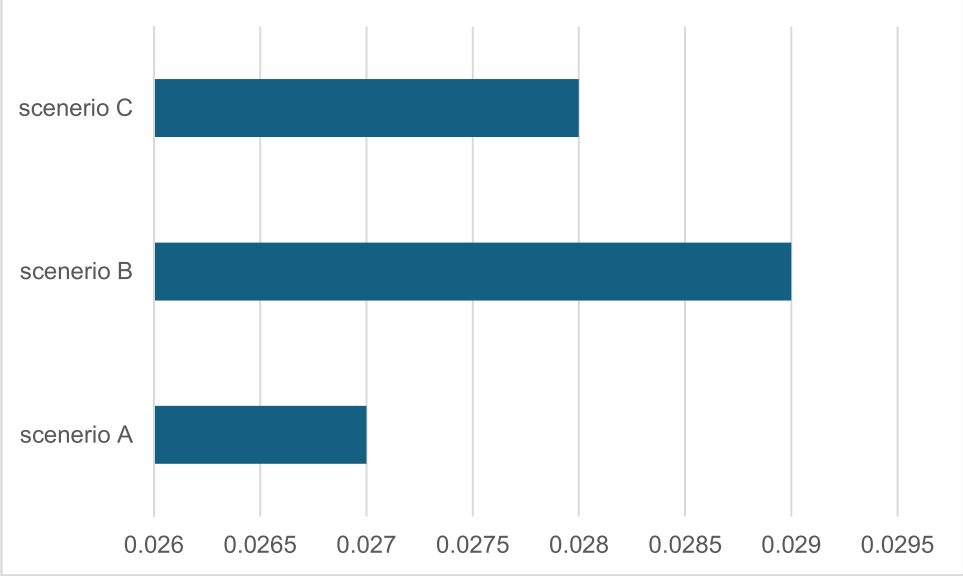

Fig. 3.7. Comparison of configuration based on LCOE.

environmental footprint, reducing lifecycle greenhouse gas emissions by 51–90%, and avoids the extraction-related risks such as soil degradation, air pollution, and water contamination associated with natural gas production. The optimization results revealed that, when compared to the other proposed hybrid energy systems in this study, the hybrid PV/wind/pumped hydro/battery/biogas system is the

Table 3.15. Summary of the system comparison.

SYSTEM(S)	Initial Capital Cost *Ck* ($)	O & M Cost ($)	Replacement Cost $	Fuel cost $	Salvage Cost $	Net Present Cost ($/yr.)	LCOE $/kWh
PV/Wind/Pumped Hydro/Battery/Biogas	2,792,000	44,065	377,943	28,589.5	148,522.0	3,085,675	0.027
PV/Wind/Battery	3,100,000	61,500	205,882	0.0	108,768.0	3,258,614	0.029
Wind/Pumped Hydro/Biogas	2,340,000	98,550	558,481	60,159.0	28,901.4	3,220,895	0.028

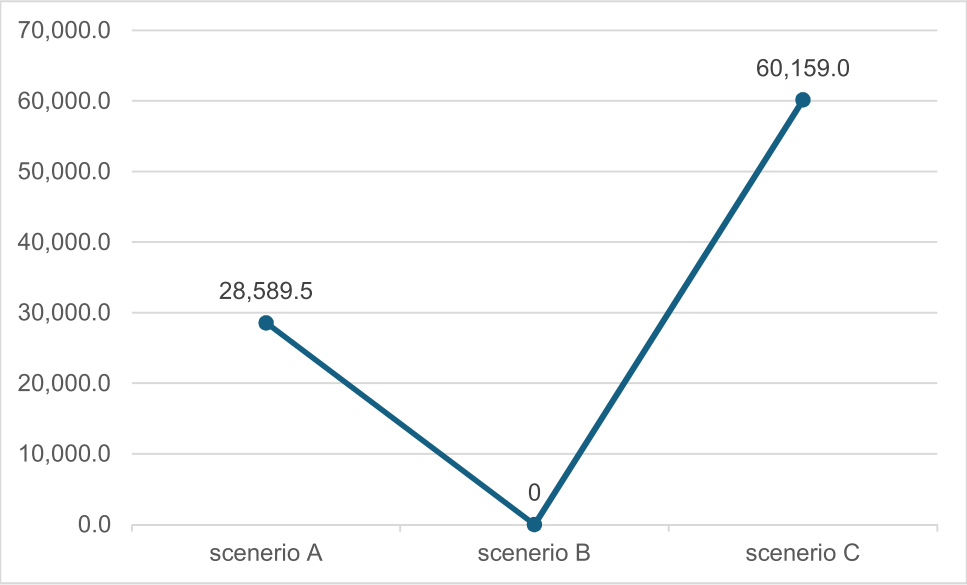

Fig. 3.8. Comparison of configuration based on fuel cost.

most techno-economically optimal choice for the current study site, resulting in the lowest NPC and LCOE of $3,085,675 and 0.027 $/kW. It was found that the system is dependable and cost-effective, as it can supply electricity at the lowest possible cost. This proposed configuration can effectively meet the load demand with no load shortage. So, the proposed system can be feasible for an off-grid situation. This hybrid system is intended to address the intermittent nature and high upfront cost of RE while reducing the fuel consumption and high cost of biogas alone, increasing the dependability, affordability, and sustainability of rural electricity supply.

The proposed PV–wind–biogas–storage HRES achieves a net present cost of 3.09M$ and a levelized cost of energy of 0.027$/kWh, with capital and replacement costs dominating the lifecycle expenditure. In the literature, similar hybrid systems for rural and remote applications typically report NPC values between about $0.3M and $6.8M and LCOE values in the range 0.18–0.33$/kWh, depending on configuration, scale, and biogas dependence. The significantly lower LCOE obtained in this study, therefore, indicates that the proposed configuration is highly competitive in terms of specific energy cost, despite its relatively high NPC driven by the use of multiple renewable and storage technologies. At the same time, the inclusion of biogas and dual storage (battery and pumped hydro) provides full renewable coverage and higher reliability than simpler PV–battery systems, justifying the investment profile shown in the comparison Table 3.16 below.

3.8. Sensitive analysis

A sensitivity study was conducted to assess the impact of variations in solar and wind resources (±10–20%) on system performance. The results indicate that dispatch patterns remained largely

Table 3.16. NPC and LCOE comparison between the proposed HRES and literature studies.

STUDY	CONFIGURATION	CONTENT	NPC	LCOE	REMARK
[32]	PV/WT/BAT/CONV/DG	Remote community	6.81M$	0.319$/kWh	Includes diesel backup; higher NPC but firm supply
[33]	PV/Battery	Rural off-grid	0.33M$	0.18$/kWh	Simple two-source system with storage only
[34]	PV/WT/Battery	Nigerian context	–	0.20–0.30$/kWh	Shows strong cost benefit of PV-based hybrids
[24]	PV/WT/Storage	Standalone HRES	–	0.22$/kWh	Optimized design for minimum LCOE
This work	PV/WT/Biogas/Battery–Inverter/Pumped hydro	Standalone rural microgrid	3.09M$	0.027$/kWh	100% renewable supply with dispatchable biogas

stable across this range, with only minor impacts on reliability and cost. However, when solar or wind availability decreased by more than 25%, the system increased its reliance on the biogas generator, which had a slight impact on overall reliability. These findings demonstrate that the proposed design is robust against moderate fluctuations in renewable generation, future work will explore more advanced methods, such as stochastic optimization, to further mitigate the effects of resource variability. The battery supplies the load while the (PPHS) gathers momentum, and the priority given to the (PPHS) ensures that the battery charging and discharging cycles are kept low. Hence, the life span of battery storage can be prolonged.

The scheduling algorithm was able to reduce the contribution of the biogas generator to less than 50% of the total load demand for 8 out of the 10 considered scenarios. Moreover, the dispatch logic reduced the frequency and depth of battery cycling, consistent with literature showing that optimized scheduling can significantly extend battery life. These findings resonate with field studies in hybrid rural microgrids, where coordinated renewable dispatch minimized generator runtime while maintaining reliability, [35, 36]. Collectively, the results affirm the feasibility of the proposed design and its viability as a cost-effective, resilient solution for rural microgrid applications.

The SQP routine was implemented and tested in MATLAB/Simulink, where it converged within approximately 1–2 seconds per dispatch interval. This level of computational performance is well within the range required for typical microcontroller-based or embedded platforms, indicating that the approach is suitable for real-time applications. The robustness of the proposed SQP-based intelligent coordination strategy was evaluated using a deterministic scenario-based validation approach. The optimization was performed over five representative daily operating scenarios, each characterized by distinct load demand profiles that show typical weekday variations. Across all scenarios, the SQP algorithm consistently converged while strictly satisfying operational and power balance constraints. The resulting economic and reliability indicators, including LCOE and NPC, showed minimal variation between scenarios, indicating stable and repeatable performance under varying load conditions. Furthermore, a one-at-a-time sensitivity analysis with $\pm 20\%$ variation in key system parameters demonstrated that the proposed coordination strategy maintains reliable operation and economic viability, highlighting the suitability of SQP for constrained optimization in hybrid renewable energy systems.

Compared with heuristic algorithms such as GA and PSO, which rely on stochastic population-based searches and typically require many function evaluations, Sequential Quadratic Programming (SQP) offers faster and more reliable convergence for constrained nonlinear problems. SQP exploits gradient information and explicitly enforces operational constraints at each iteration, leading to improved computational efficiency and solution accuracy. These characteristics make SQP particularly suitable for repeated, scenario-based coordination of hybrid renewable energy systems where timely and feasible solutions are required.

Although demonstrated on the Obafemi Awolowo University microgrid, the proposed SQP-based coordination framework is general and scalable. Its modular component modeling and parameterized inputs allowed straightforward adaptation to hybrid renewable energy systems of different sizes, configurations, and load/resource conditions without changing the underlying optimization structure.

The proposed intelligent coordination strategy is currently validated through MATLAB-based simulations, which enable controlled evaluation of system performance under diverse operating scenarios. While simulation provides valuable insights into feasibility and comparative performance, further validation using hardware-in-the-loop (HIL) or prototype-level testing would strengthen the practical applicability of the approach. Future work will therefore focus on implementing the coordination algorithm on real-time simulation platforms (e.g., HIL environments) and small-scale experimental HRES prototypes to assess computational latency, communication delays, and robustness under real-world disturbances. Such experimental validation will provide additional confidence in the scalability and deployment readiness of the proposed system.

4. Conclusion

This work presented an intelligent coordination and optimal sizing framework for a hybrid renewable energy system composed of wind, solar PV, pumped hydro, battery–inverter, and biogas units. The proposed SQP-based optimization minimized the system net present cost while satisfying power balance, storage, and operational constraints, resulting in a total NPC of 3.09M$ and an LCOE of 0.027$/kWh over 26.5 years. This study further demonstrated that the proposed intelligent, microcontroller-based coordination framework can effectively manage the off-grid HRES, improving energy efficiency and substantially reducing reliance on backup biogas generation (by

about 70% in the simulated scenarios). The integration of pumped-hydro storage enhanced overall system performance, achieving a load-supply reliability greater than 99% under varying seasonal operating conditions. Overall, the analysis showed that capital and replacement costs dominate the lifecycle expenditure, with solar PV and biogas accounting for the largest share of NPC, while O&M and fuel costs remain relatively small; the coordination strategy ensured a reliable supply for the academic-session load profile by effectively exploiting the complementary characteristics of intermittent (PV/wind), dispatchable (biogas), and storage (battery/pumped hydro) resources.

A key contribution of the study is the development of an intelligent coordination strategy based on a mathematically rigorous, gradient-based SQP algorithm to solve the HRES sizing problem with exact constraint handling and fast convergence, offering a deterministic alternative to heuristic methods such as GA and PSO, which are typically more computationally demanding. The developed framework integrates detailed cost modelling (capital, O&M, replacement, salvage, and biogas fuel) with realistic load data, providing a techno-economic benchmark that can be directly compared with existing hybrid system designs. However, the approach assumes deterministic resource and load profiles, idealized component behaviour, and model parameters derived from literature and vendor data, which may not fully capture all uncertainties and degradation mechanisms present in real-world installations.

Future work

Future research will focus on extending the present framework toward real-time deployment and more advanced control strategies. First, incorporating predictive scheduling based on short-term forecasts of solar irradiance, wind speed, and demand will enable model-predictive operation that can further reduce operating costs and improve reliability under uncertainty. Second, integrating real-time sensing and communication infrastructure—such as smart meters, weather stations, and condition-monitoring units—will allow the coordination algorithm to adapt online to component ageing, unexpected demand variations, and equipment faults.

Additional extensions include coupling the SQP-based planner with higher-level energy management schemes (for example, hierarchical or hybrid intelligent controllers) that can coordinate multiple microgrids or interact with the main grid under time-varying tariffs. Experimental validation through hardware-in-the-loop tests deployment on the target campus is also envisaged to verify the performance of the control strategy under practical constraints such as measurement noise, communication delays, and non-ideal switching behaviour.

Acknowledgments

I acknowledge the support of Prof. O. O. Jegede of the Atmospheric Physics Research Group of the Department of Physics and Engineering Physics and Dr. O. J. Matthew of the Space Application and Environmental Science Laboratory, SPAEL in the Institute of Ecology and Environmental Studies; Engineer Olawoyin of the powerhouse, OAU, Ile–Ife, for the provision of the data needed for the research.

Data availability statement

All data generated or analyzed during this study are included in this published article. Additional datasets related to the MATLAB code are available from the corresponding author upon reasonable request.

Conflicts of interest

The authors declare that there are no conflicts of interest regarding the publication of this paper.

Author contributions

Conceptualization, methodology, formal analysis, Writing – review & editing, software**: Joseph Bukola Samson;** Conceptualization, Methodology, Supervision, Writing – review & editing. **Olufisayo Stephen Babalola;** Conceptualization, investigation, software: **Olatunji Waliu Olademeji;** formal analysis, investigation, software, validation, Writing – review & editing: **Samson Oladayo Ayanlade;** formal analysis, methodology, software, visualization: **Etinosa Noma-Osaghae**; formal analysis, investigation, methodology, Writing – review & editing: **Opeyemi Ahmed Ajibola.** All authors have read and agreed to the published version of the manuscript.

Funding

No specific grant was received for this research from any funding agency in the public, commercial, or not-for-profit sectors, or conflict of interest: none declared.

References

1. J. Shrestha, *Rural Road Development in Developing Countries*: Springer Nature, 2025 ISBN 9789819620111, https://doi.org/10.1007/978-981-96-2012-8.
2. D. J. Soeder and D. J. Soeder, "Fossil fuels and climate change," *Fracking and the Environment: A scientific assessment of the environmental risks from hydraulic fracturing and fossil fuels,* pp. 155–185, 2021.
3. A. Al Ezzi, M. T. Chaichan, H. S. Majdi, A. H. Al-Waeli, H. A. Kazem, K. Sopian, *et al.*, "Nano-iron oxide-ethylene glycol-water nanofluid based photovoltaic thermal (PV/T) system with spiral flow absorber: An energy and exergy analysis," *Energies,* vol. 15, p. 3870, 2022.
4. M. T. Chaichan, M. T. Mahdi, H. A. Kazem, A. H. Al-Waeli, M. A. Fayad, A. A. Al-Amiery, *et al.*, "Modified nano-Fe2O3-paraffin wax for efficient photovoltaic/thermal system in severe weather conditions," *Sustainability,* vol. 14, p. 12015, 2022.
5. O. J. Olujobi, U. E. Okorie, E. S. Olarinde, and A. D. Aina-Pelemo, "Legal responses to energy security and sustainability in Nigeria's power sector amidst fossil fuel disruptions and low carbon energy transition," *Heliyon,* vol. 9, 2023.
6. S. Algarni, V. Tirth, T. Alqahtani, S. Alshehery, and P. Kshirsagar, "Contribution of renewable energy sources to the environmental impacts and economic benefits for sustainable development," *Sustainable energy technologies and assessments,* vol. 56, p. 103098, 2023.
7. P. Gajewski and K. Pieńkowski, "Control of the hybrid renewable energy system with wind turbine, photovoltaic panels and battery energy storage," *Energies,* vol. 14, p. 1595, 2021.
8. M. Hamidi, A. Raihani, and O. Bouattane, "Sustainable intelligent energy management system for microgrid using multi-agent systems: A case study," *Sustainability,* vol. 15, p. 12546, 2023.
9. K. Ukoba, K. O. Olatunji, E. Adeoye, T.-C. Jen, and D. M. Madyira, "Optimizing renewable energy systems through artificial intelligence: Review and future prospects," *Energy & Environment,* vol. 35, pp. 3833–3879, 2024.
10. M. Amir, Zaheeruddin, and A. Haque, "Intelligent based hybrid renewable energy resources forecasting and real time power demand management system for resilient energy systems," *Science Progress,* vol. 105, p. 00368504221132144, 2022.
11. M. E. Shayan, G. Najafi, B. Ghobadian, S. Gorjian, and M. Mazlan, "A novel approach of synchronization of the sustainable grid with an intelligent local hybrid renewable energy control," *International Journal of Energy and Environmental Engineering,* vol. 14, pp. 35-46, 2023/03/01 2023.
12. M. Cavus, "Advancing Power Systems with Renewable Energy and Intelligent Technologies: A Comprehensive Review on Grid Transformation and Integration," *Electronics,* vol. 14, p. 1159, 2025.
13. N. Kanagaraj, M. Vijayakumar, M. Ramasamy, and O. Aldosari, "Energy management and power quality improvement of hybrid renewable energy generation system using coordinated control scheme," *IEEE Access,* vol. 11, pp. 93254–93267, 2023.
14. M. Khalil and S. A. Sheikh, "Advancing Green Energy Integration in Power Systems for Enhanced Sustainability: A Review," *IEEE Access,* 2024.
15. I. E. Atawi, A. Q. Al-Shetwi, A. M. Magableh, and O. H. Albalawi, "Recent advances in hybrid energy storage system integrated renewable power generation: Configuration, control, applications, and future directions," *Batteries,* vol. 9, p. 29, 2022.
16. M. Cheng, X. Zhao, M. Dhimish, W. Qiu, and S. Niu, "A Review of Data-driven Surrogate Models for Design Optimization of Electric Motors," *IEEE Transactions on Transportation Electrification,* 2024.
17. S. G. Malla, J. M. R. Malla, P. Malla, S. Ramasamy, S. K. Doniparthi, M. K. Sahu, *et al.*, "Coordinated power management and control of renewable energy sources based smart grid," *International Journal of Emerging Electric Power Systems,* vol. 23, pp. 261–276, 2022.
18. P. Arévalo and F. Jurado, "Impact of artificial intelligence on the planning and operation of distributed energy systems in smart grids," *Energies,* vol. 17, p. 4501, 2024.
19. M. S. Bakare, A. Abdulkarim, A. N. Shuaibu, and M. M. Muhamad, "Energy management controllers: strategies, coordination, and applications," *Energy Informatics,* vol. 7, p. 57, 2024.
20. P. Biswas, A. Rashid, A. Al Masum, M. A. Al Nasim, A. A. Ferdous, K. D. Gupta, *et al.*, "An extensive and methodical review of smart grids for sustainable energy management-addressing challenges with ai, renewable energy integration and leading-edge technologies," *IEEE Access,* 2025.
21. A. Vincent, "Optimal Energy Management System for PV/Wind/Diesel-Battery Power Systems for Rural Health Clinic," *International Journal of Intelligent Systems and Applications in Engineering,* vol. 2, pp. 64–70, 2014.
22. M. Bruck, P. Sandborn, and N. Goudarzi, "A Levelized Cost of Energy (LCOE) model for wind farms that include Power Purchase Agreements (PPAs)," *Renewable Energy,* vol. 122, pp. 131–139, 2018.
23. T. Stehly, P. Duffy, and D. Mulas Hernando, "2022 cost of wind energy review [slides]," National Renewable Energy Laboratory (NREL), Golden, CO (United States)2023.
24. Y. Ayed, R. Al Afif, P. Fortes, and C. Pfeifer, "Optimal design and techno-economic analysis of hybrid renewable energy systems: A case study of Thala city, Tunisia," *Energy Sources, Part B: Economics, Planning, and Policy,* vol. 19, p. 2308843, 2024.
25. X. Xu, X. Xu, S. Li, X. Zhang, Z. Xu, T. Ma, *et al.*, "Simulation and optimization of hybrid renewable energy system to achieve a net-zero and flexible-interconnected service area for highways," *Energy for Sustainable Development,* vol. 87, p. 101740, 2025.
26. M. Xiong, F. Gao, K. Liu, S. Chen, and J. Dong, "Optimal real-time scheduling for hybrid energy storage systems and wind farms based on model predictive control," *Energies,* vol. 8, pp. 8020–8051, 2015.
27. B. Zhang, "Modelling and Optimization of Multi-Energy System Operation Based on Deep Reinforcement Learning," 2024.
28. I. Adebayo, Y. Sun, and U. Awal, "Economic optimization of hybrid renewable energy resources for rural electrification," *International Journal of Power Electronics and Drive Systems (IJPEDS),* vol. 15, pp. 1147–1157, 2024.
29. S. O. Sanni, J. Y. Oricha, T. O. Oyewole, and F. I. Bawonda, "Analysis of backup power supply for unreliable grid using hybrid solar PV/diesel/biogas system," *Energy,* vol. 227, p. 120506, 2021.
30. M. Naumann, R. C. Karl, C. N. Truong, A. Jossen, and H. C. Hesse, "Lithium-ion battery cost analysis in PV-household application," *Energy Procedia,* vol. 73, pp. 37–47, 2015.
31. V. Mudgal, K. Reddy, and T. Mallick, "Techno-economic analysis of standalone solar photovoltaic-wind-biogas hybrid renewable energy system for community energy requirement," *Future cities and environment,* vol. 5, 2019.
32. Y. W. Koholé, C. A. W. Ngouleu, F. C. V. Fohagui, and G. Tchuen, "Optimization and comparative analysis of hybrid

renewable energy systems for sustainable and clean energy production in rural Cameroon considering the loss of power supply probability concept," *Energy Conversion and Management: X,* vol. 25, p. 100829, 2025.

33. A. I. Hassane, D. H. Didane, A. M. Tahir, R. M. Mouangue, J. G. Tamba, and J.-M. Hauglustaine, "Comparative analysis of hybrid renewable energy systems for off-grid applications in chad," *International Journal of Renewable Energy Development,* vol. 11, p. 49, 2022.
34. A. A. Mas' ud, A. Yunusa-Kaltungo, N. A. Rufa'I, and N. Yusuf, "Assessing the viability of hybrid renewable energy systems in Nigeria," *Engineering Reports,* vol. 6, p. e12979, 2024.
35. F. Canziani, R. Vargas, and J. A. Gastelo-Roque, "Hybrid photovoltaic-wind microgrid with battery storage for rural electrification: a case study in perú," *frontiers in energy research,* vol. 8, p. 528571, 2021.
36. J. E. C. Saire, J. A. Gastelo-Roque, and F. Canziani, "Study of a hybrid photovoltaic-wind smart microgrid using data science approach," in *2021 IEEE PES Innovative Smart Grid Technologies Conference-Latin America (*ISGT Latin America*)*, 2021, pp. 1–5.